F I N A L   R E P O R T

SCREENING / SCOPING LEVEL PROBABILISTIC SEISMIC HAZARD ANALYSES

GRANITE REEF DIVERSION AND THEODORE ROOSEVELT DAMS

SALT RIVER PROJECT SOUTHERN ARIZONA

Prepared for

U.S. Department of the Interior
Bureau of Reclamation
Denver, Colorado

18 December 2002

URS Corporation
Seismic Hazards Group
500 12th Street, Suite 200
Oakland, California 94607

TABLE OF CONTENTS

Tables

Figures

TABLE OF CONTENTS

SCREENING / SCOPING LEVEL PROBABILISTIC SEISMIC HAZARD ANALYSES

GRANITE REEF DIVERSION AND THEODORE ROOSEVELT DAMS

Prepared for the

U.S. Department of the Interior
Bureau of Reclamation
Denver, Colorado

Prepared by

Ivan Wong, Mark Dober, Clark Fenton, Robyn Schapiro, and Eliza Nemser
Seismic Hazards Group
URS Corporation
500 12th Street, Suite 200
Oakland, California 94607

18 December 2002

This report presents the results of probabilistic seismic hazard analyses for use in screening/scoping-level dam safety and/or risk assessments of Granite Reef Diversion and Theodore Roosevelt Dams in southern Arizona (Figure 1). The purpose of these evaluations is to estimate the levels of ground motions, which will be exceeded at specified annual frequencies (or return periods), at the damsites.

Granite Reef Diversion Dam, completed in 1908, is an 8.8-m-high concrete ogee weir with embankment wings. It is located on the Salt River approximately 35 km east of Phoenix, Arizona (Figure 1). Theodore Roosevelt Dam was originally completed in 1911 as a 85-m-high cyclopean masonry thick-arch structure with a reservoir capacity of 1.70 x 10^9 m^3 (1,381,580 acre-feet). Modifications completed in 1996 consisted principally of placing a concrete overlay on the existing masonry dam and raising the crest 23.5 m. The dam is located on the Salt River, about 122 km northeast of Phoenix.

In this study, the available geologic and seismologic data, including seismotectonic investigations previously performed by Reclamation (Anderson *et al.*, 1986; 1987; Piety and Anderson, 1990), and by URS Greiner Woodward-Clyde (URSGWC) for Bartlett, Horseshoe, New Waddell, and Stewart Mountain Dams (Wong *et al.*, 2000), were used to evaluate and characterize potential seismic sources, the likelihood of earthquakes of various magnitudes occurring on those sources, and the likelihood of the earthquakes producing ground motions over a specified level. Our evaluation was limited in scope, relying solely on available data and information. Thus no field investigations were performed. The uncertainties in seismic source characterization, which are sometimes quite large for the lesser studied faults, reflect the quality of the available information.

The probabilistic seismic hazard analysis methodology used in this study allows for the explicit inclusion of the range of possible interpretations in components of the model, including seismic source characterization and ground motion estimation. Uncertainties in models and parameters are incorporated into the hazard analyses through the use of logic trees. The following presents the seismic source characterization, the attenuation relationships used in the probabilistic analyses of the two dams, and the hazard results.

1.1 ACKNOWLEDGMENTS

The probabilistic seismic hazard analyses of these two dams were performed by the following personnel of URS Corporation:

Seismic Source Characterization	Dr. Clark Fenton, Mark Dober, and Ivan Wong
Probabilistic Analyses	Mark Dober and Ivan Wong
Report Preparation	Ivan Wong, Robyn Schapiro, and Eliza Nemser

Ivan Wong was the Project Manager. Our thanks to Dr. Jon Ake, Larry Anderson, Fred Hawkins, and Roland LaForge of Reclamation for their assistance. Our appreciation to Marilyn Mackel and Fumiko Goss for their assistance in the preparation of this report.

The seismic hazard approach used in this study is based on the model developed principally by Cornell (1968) and McGuire (1974; 1978). The occurrence of earthquakes on a fault is assumed to be a Poisson process. The Poisson model is widely used and is a reasonable assumption in regions where data are sufficient to provide only an estimate of average recurrence rate (Cornell, 1968). When there are sufficient data to permit a real-time estimate of the occurrence of earthquakes, the probability of exceeding a given value can be modeled as an equivalent Poisson process in which a variable average recurrence rate is assumed. The occurrence of ground motions at the site in excess of a specified level also is a Poisson process, if (1) the occurrence of earthquakes is a Poisson process, and (2) the probability that any one event will result in ground motions at the site in excess of a specified level is independent of the occurrence of other events.

The probability that a ground motion parameter "Z" exceeds a specified value "z" in a time period "t" is given by:

$$p(Z > z) = 1-e^{-\nu(z)\bullet t} \qquad (1)$$

where $\nu(z)$ is the annual mean number (or rate) of events in which Z exceeds z. It should be noted that the assumption of a Poisson process for the number of events is not critical. This is because the mean number of events in time t, $\nu(z)\bullet t$, can be shown to be a close upper bound on the probability $p(Z > z)$ for small probabilities (less than 0.10) that generally are of interest for engineering applications. The annual mean number of events is obtained by summing the contributions from all sources, that is:

$$\nu(z) = \sum_n \nu_n(z) \qquad (2)$$

where $\nu_n(z)$ is the annual mean number (or rate) of events on source n for which Z exceeds z at the site. The parameter $\nu_n(z)$ is given by the expression:

$$\nu_n(z) = \sum_i \sum_j ß_n(m_i) \bullet p(R=r_j|m_i) \bullet p(Z>z|m_i,r_j) \qquad (3)$$

where:

$ß_n(m_i)$ = annual mean rate of recurrence of earthquakes of magnitude increment m_i on source n;

$p(R=r_j|m_i)$ = probability that given the occurrence of an earthquake of magnitude m_i on source n, r_j is the closest distance increment from the rupture surface to the site;

$p(Z > z|m_i,r_j)$ = probability that given an earthquake of magnitude m_i at a distance of r_j, the ground motion exceeds the specified level z.

The calculations were made using the computer program HAZ20 developed by N. Abrahamson.

2.1 SEISMIC SOURCE CHARACTERIZATION

Two types of earthquake sources are characterized in this seismic hazard analysis: (1) fault sources; and (2) areal source zones (Section 3.1). Fault sources are modeled as three-dimensional fault surfaces and details of their behavior are incorporated into the source characterization. Areal source zones are regions where earthquakes are assumed to occur randomly. Seismic sources are modeled in the hazard analysis in terms of geometry and earthquake recurrence.

The geometric source parameters for faults include fault location, segmentation model, dip, and thickness of the seismogenic zone. The recurrence parameters include recurrence model, recurrence rate (slip rate or average recurrence interval for the maximum event), slope of the recurrence curve (*b*-value), and maximum magnitude. Clearly, the geometry and recurrence are not totally independent. For example, if a fault is modeled with several small segments instead of large segments, the maximum magnitude is lower, and a given slip rate requires many more small earthquakes to accommodate a cumulative seismic moment. For areal source zones, only the areas, maximum magnitude, and recurrence parameters (based on the historical earthquake record) need to be defined.

Uncertainties in the source parameters are included in the hazard model using logic trees (Figure 2). In the logic tree approach, discrete values of the source input parameters have been included along with our estimate of the likelihood that the discrete value represents the actual value. In this probabilistic analysis, generally all input parameters have been represented by three values; the values represent a distribution about the best estimate (Figure 2).

2.1.1 Source Geometry

In the probabilistic analysis, it is assumed that earthquakes of a certain magnitude may occur randomly along the length of a given fault or segment. The distance from an earthquake to the site is dependent on the source geometry, the size and shape of the rupture on the fault plane, and the likelihood of the earthquake occurring at different points along the fault length. The distance to the fault is defined to be consistent with the specific attenuation relationship used to calculate the ground motions. The distance, therefore, is dependent on both the dip and depth of the fault plane, and a separate distance function is calculated for each geometry and each attenuation relationship. The size and shape of the rupture on the fault plane are dependent on the magnitude of the earthquake, with larger events rupturing longer and wider portions of the fault plane. We modeled the rupture dimensions following the magnitude-rupture length relationship of Wells and Coppersmith (1994).

2.1.2 Fault Recurrence

The recurrence relationships for the faults are modeled using the exponentially truncated Gutenberg-Richter relationship, characteristic earthquake, and maximum magnitude recurrence models. These models are weighted (Figure 2) to represent our judgment on their applicability to the sources. For the areal source zones, only an exponential recurrence relationship is assumed appropriate.

We have used the general approach of Molnar (1979) and Anderson (1979) to arrive at the recurrence for the exponentially truncated model. The model where faults rupture with a "characteristic" magnitude on specific segments has been included. This model is described by Aki (1983) and Schwartz and Coppersmith (1984). We have used the numerical model of Youngs and Coppersmith (1985) for the characteristic model. The number of events exceeding a given magnitude, $N(m)$, for the truncated exponential relationship is:

$$N(m) = \alpha(m^o)\frac{10^{-b(m-m^o)} - 10^{-b(m^u-m^o)}}{1-10^{-b(m^u-m^o)}} \tag{4}$$

where $\alpha(m^o)$ is the annual frequency of occurrence of earthquakes greater than the minimum magnitude, m^o; b is the Gutenberg-Richter parameter defining the slope of the recurrence curve; and m^u is the upper-bound magnitude event that can occur on the source. A m^o of moment magnitude (**M**) 5 was used for the hazard calculations because smaller events are not considered likely to produce ground motions with sufficient energy to damage well designed structures.

The model that the faults rupture with a "characteristic" magnitude on specific segments has been included. This model is described by Aki (1983) and Schwartz and Coppersmith (1984). We have used the numerical model of Youngs and Coppersmith (1985) for the characteristic model. For the characteristic model, the number of events exceeding a given magnitude is the sum of the characteristic events and the non-characteristic events. The characteristic events are distributed uniformly over ± 0.3 magnitude unit around the characteristic magnitude and the remainder of the moment rate is distributed exponentially using the above equation with a maximum magnitude one unit lower than the characteristic magnitude (Youngs and Coppersmith, 1985).

The maximum magnitude model can be regarded as an extreme version of the characteristic model. We adopted the model proposed by Wesnousky (1986). In the maximum magnitude model, there is no exponential portion of the recurrence curve, i.e., no events can occur between the minimum magnitude of **M** 5.0 and the distribution about the maximum magnitude.

The recurrence rates for the fault sources are defined by either the slip rate or the average return time for the maximum or characteristic event and the recurrence *b*-value. The slip rate is used to calculate the moment rate on the fault using the following equation defining the seismic moment:

$$M_o = \mu\, A\, D \tag{5}$$

where M_o is the seismic moment, μ is the shear modulus, A is the area of the rupture plane, and D is the slip on the plane. Dividing both sides of the equation by time results in the moment rate as a function of slip rate:

$$\dot{M}_o = \mu\, A\, S \tag{6}$$

where $\dot{M}_o$ is the moment rate and S is the slip rate. M_o has been related to **M** by Hanks and Kanamori (1979):

$$M_w = 2/3 \log M_o - 10.7 \tag{7}$$

Using this relationship and the relative frequency of different magnitude events from the recurrence model, the slip rate can be used to estimate the absolute frequency of different magnitude events.

The average return time for the characteristic or maximum magnitude event defines the high magnitude (low likelihood) end of the recurrence curve. When combined with the relative frequency of different magnitude events from the recurrence model, the recurrence curve is established.

2.2 ATTENUATION RELATIONSHIPS

To characterize the ground motions at a specified site as a result of the seismic sources considered in the probabilistic seismic hazard analysis, empirical attenuation relationships for spectral accelerations are used. The relationships used in this study were selected on the basis of the appropriateness of the site conditions and tectonic environment for which they were developed (Figure 2).

The uncertainty in ground motion attenuation was included in the probabilistic analysis by using the log-normal distribution about the median values as defined by the standard error associated with each attenuation relationship. Three standard deviations about the median value were included in the analysis.

The following section discusses the characterization of the seismic sources considered in the probabilistic seismic hazard analyses and the empirical attenuation relationships selected and used.

3.1 SEISMOTECTONIC SETTING

Granite Reef Diversion and Theodore Roosevelt Dams are located within the Colorado Plateau – Basin and Range Transition Zone in central Arizona. The Transition Zone separates the southern Colorado Plateau to the north and the southern Basin and Range Province to the south. All three regions are characterized by relatively few late Quaternary faults and low rates of seismicity. These regions are bounded to the west by the Salton Trough Province, a region characterized by right-lateral strike-slip faulting and elevated levels of contemporary seismicity.

The Transition Zone is characterized by north- to northwest-trending mountain ranges and intervening valleys or basins, that are the result of Miocene normal faulting. The topography of the Transition Zone is more subdued than that of the southern Basin and Range Province to the south, with the ranges being less pronounced and the basins being smaller and less well defined. Bedrock in the region consists primarily of Precambrian metamorphic and granitic plutonic rocks and Paleozoic sediments. Basin-fill sediments are late Cenozoic in age, and clast composition reflects widespread Tertiary volcanism in the region. Several Quaternary normal faults are mapped in the region. Based on reconnaissance mapping and limited paleoseismic studies, these faults have average recurrence intervals of tens to hundreds of thousands of years (Pearthree, 1998; Piety and Anderson, 1991). The historical record indicates low to moderate levels of seismicity (Brumbaugh, 1987; Bausch and Brumbaugh, 1997).

The southern Basin and Range Province is characterized by a block-faulted topography of alternating mountain range blocks bounded by moderately to steeply-dipping normal faults and intervening valleys. The mountains comprise igneous, metamorphic, and indurated sedimentary rocks of Precambrian through Tertiary age, while the valleys are filled with a relatively undeformed sequence of fluvial and lacustrine sediments of Oligocene to Pleistocene age. The present-day structural basins resulted from a period of extensive normal faulting, the Basin and Range disturbance, that began 10 to 13 Ma. Landforms indicating tectonic inactivity dominate the region today, implying cessation of major extension at some time in the late Miocene or Pliocene (Menges and McFadden, 1981). This is reflected by the low levels of historical seismicity and sparse evidence for Quaternary faulting in southern Arizona. The southern Basin and Range Province is dominated by northwest-southeast-striking normal faults; however, the study area encompasses the transition from this northwest-southeast structural grain to a more north-south orientation as the province extends into northern Mexico.

The Colorado Plateau is an area of relative tectonic stability surrounded by active extensional seismotectonic provinces. Although there is a lack of major crustal deformation since the end of Laramide orogeny (40 Ma), the Colorado Plateau has been subject to about 2 km of epeirogenic uplift in the Cenozoic (Morgan and Swanberg, 1985). During uplift, the plateau acted as a coherent block, with only minor differential movements creating northerly-trending monoclines and associated structural basins. This is a region of elevated topography comprising dissected plateau areas. Contemporary seismicity is characterized as being low to moderate, with widespread, generally small events that cannot be correlated with surface geological features (Wong and Humphrey, 1989).

The Salton Trough is an area of transition between ocean-floor spreading of the Gulf of California and right-lateral strike-slip faulting of the San Andreas fault zone. This region, forming the southwestern extremity of the study region, is one of the most seismically active areas in the western United States with repeated events of **M** 6 to 7 during historical time. The Salton Trough is a structural basin filled with deltaic sediments from the Colorado River and bounded to the northeast by dissected metasedimentary highlands. Slip rates on faults in this region are as high as 30 mm/yr (Working Group on California Earthquake Potential, 1995).

3.2 SEISMIC SOURCES

The following discusses the faults and areal (background earthquake) source zone characterized as seismic sources in the probabilistic analysis.

3.2.1 Faults

Three faults within a distance of about 100 km from the damsites were considered in this evaluation. They included the Horseshoe, Carefree, and Sugarloaf faults within the Transition Zone. These faults were considered in the analysis because they could contribute to the probabilistic ground shaking hazard at each damsite due to their maximum earthquakes and distances from the damsites. Although they are quite distant, the southern San Andreas fault and the Pitaycachi fault in the southern Basin and Range Province were also considered in the hazard analysis because of their potential to generate very large events (**M** 8 and 7.5, respectively) compared to the local faults.

Each of these faults was characterized in terms of its maximum earthquake, fault geometry, and earthquake recurrence based on previous investigations by Reclamation (Anderson *et al.*, 1986, 1987; Ertec, 1981; Piety and Anderson, 1990) and available published data (Pearthree, 1998). Table 1 summarizes the fault source parameters used in this analysis and Figure 3 shows the locations of all of the faults.

Unless there is evidence to suggest otherwise, all faults are included as single, independent (unsegmented), planar sources. However, it should be noted that the rupture behavior of most of these faults is either poorly understood or unknown. Actual fault behavior may be more complex than what we have assumed in this analysis. With the exception of the right-lateral, strike-slip San Andreas fault, all faults are normal, dip-slip faults. For both segmented and independent sources, we have adopted a preferred dip of 60 ± 15° typical for range-bounding normal faults in the western U.S. (Doser and Smith, 1989).

Fault activity is characterized by probability of activity and slip rate. In assigning probabilities of activity for the fault sources, we considered the likelihood that the structure is capable of independently generating an earthquake, i.e., that it is potentially seismogenic, and the likelihood that it is still active within the neotectonic stress regime. Many factors were used in these determinations including: fault orientation with respect to the contemporary stress regime, fault geometry, relation to other seismogenic structures, age of youngest movement, rates of activity, geomorphic expression, amount of cumulative offset, and evidence for a non-tectonic origin. Generally, faults with definitive evidence of Holocene displacement or repeated late Quaternary (post-middle Pleistocene) activity were assigned a probability of activity of 1.0. All other faults were judged on an individual basis.

All available data were incorporated in developing slip rate distributions for the faults in this analysis. Where the data were available, we used late Pleistocene or younger offsets to calculate the slip rates. However, in most cases we have had to use longer term slip rates, mainly calculated from displacements of lower and middle Quaternary, but also upper Tertiary strata. Where displacement data have been absent for suspected active faults, we have assigned the slip rate distributions from faults with apparently similar levels of activity (as determined by similarities in geomorphic expression).

Fault locations and lengths were taken from the sources referenced in Table 1. The magnitude of the maximum earthquake of each fault was estimated from the empirical relationship of Wells and Coppersmith (1994) between **M** and surface rupture length (SRL), for all fault types, where:

$$\mathbf{M} = 1.16*\log(\mathrm{SRL}) + 5.08$$

We considered the truncated exponential, maximum-magnitude, and characteristic recurrence models. Observations of historical seismicity and paleoseismic investigations suggest that characteristic behavior is more likely for individual faults, whereas seismicity in zones best fits a truncated exponential model (Schwartz and Coppersmith, 1984). Therefore, we favored the characteristic model (weighted 0.60) over the exponential and maximum magnitude models (weighted 0.20 each) (Figure 2).

Horseshoe Fault

The 23-km-long Horseshoe fault is located at the base of the steep, east-facing range front immediately west of Horseshoe Reservoir (Figure 3). The fault consists of two very distinct segments: the 14-km-long Hell Canyon segment that strikes north-south along the range front; and the 9-km-long Reservoir segment that strikes northwest across the reservoir basin (Piety and Anderson, 1990; 1991). Both segments of the fault show evidence of being active in about the last 10,000 to 20,000 years. Along the Hell Canyon segment, fault scarps are formed on alluvial fan deposits and also along the bedrock-alluvium contact. The Hell Canyon segment marks the boundary between crystalline basement to the west and Tertiary basin-fill sediments to the east. The alluvial scarps are 2 to 7.5 m high, indicating approximately 5 m of down-to-the-east vertical displacement. Scarp profiles indicate that the most recent event occured 15 to 30 ka. Scarp profiles also suggest that there have been two events in the last 150,000 years. A preferred slip rate of 0.02 mm/yr is calculated from 5 m displacement in 150,000 years (Pearthree, 1998).

The Reservoir segment is expressed as a low, subtle, partially-buried, north-northeast-facing fault scarp developed on a middle Pleistocene Verde River terrace. The youngest deposits displaced by this fault segment are middle and late Pleistocene in age. Based on soil development on the youngest deposit offset observed in paleoseismic trenches, the most recent faulting event occurred prior to 10 to 20 ka. Trench exposures show that there has been 1.5 to 2.0 m of down-to-the-northeast displacement of Verde River alluvium, occurring in two or possibly three events during the last 300,000 years (Piety and Anderson, 1990; 1991). The recurrence interval for these events could be 85 to 140 kyr. A slip rate of 0.01 mm/yr is calculated for no more than 2 m of vertical displacement in the last 200 to 300 kyr. We use a slip rate distribution of 0.001 to 0.2 mm/yr (Pearthree, 1998) to insure that we are encompassing all uncertainties (Table 1).

From their differing geometries and geomorphic expressions, we assume that the Hell Canyon and Reservoir segments can behave as independent rupture segments. We entertain two possible rupture scenarios: rupture of both segments together, generating a maximum earthquake of **M** 6.6 ± 0.3, and independent rupture of the Hell Canyon and Reservoir segments, each generating a maximum earthquake of **M** 6.5 ± 0.3 (Figure 4). Rupture of the entire fault is weighted slightly higher (0.6) than rupture of the individual segments (0.4). The individual segments are weighted evenly (0.5) for a segmented rupture model. The Horseshoe fault is 56 km and 50 km from Roosevelt Dam and Granite Reef Dam, respectively.

Carefree Fault

The 11-km-long Carefree fault is a north- and northwest-striking zone of normal faults along the margin of and within a pediment developed on Precambrian granite bedrock (Figure 3). The fault may displace middle Pleistocene alluvium, but upper Pleistocene and younger alluvium is not faulted. The topographic relief across the fault is less than a few meters, indicating a relatively low slip rate. The fault dips at a high angle to the west and fault scarps are low, but fairly well-defined, facing west and southwest. The fault scarps form along the bedrock-alluvium contact and reach 3 m in height. There are no unequivocal tectonic scarps formed on alluvium. According to Pearthree (1998), the most recent event is middle to late Quaternary. Total Quaternary displacement is not well defined, but is probably only several meters. A preferred slip rate of 0.03 mm/yr is calculated from 3 m of vertical displacement in the late Quaternary (Pearthree, 1998). Activity on this fault is weighted 0.7 on account of the lack of convincing evidence for late Pleistocene and Holocene movement. Due to its short rupture length of 11 km, the maximum magnitude event for the Carefree fault is considered to be **M** 6.5 ± 0.3, the minimum surface faulting magnitude. The Carefree fault is 60 km from Roosevelt Dam and 29 km from Granite Reef Dam.

Sugarloaf Fault

The Sugarloaf fault is expressed as a low, fairly continuous east-facing fault scarp up to 5 m high at the contact between Precambrian granite and Tertiary basin fill sediments along the western margin of the small sedimentary basin on the flank of the Mazatzal Mountains (Pearthree *et al.*, 1995) (Figure 3). The relief across the fault is minimal, indicating relatively little Quaternary activity (Pearthree, 1998). Stream bank exposures show down-to-the-east displacement on a northwest-striking fault plane dipping 70° to 80° to the northeast. Fault scarps on alluvium are rare and are poorly preserved. Paleoseismic trenching shows that the fault offsets late to latest Pleistocene deposits, but middle to upper Holocene deposits are not displaced (Pearthree *et al.*, 1995). The evidence for multiple Quaternary events is strong; however, the timing of individual events is poorly constrained (Pearthree *et al.*, 1995; Pearthree, 1998). A preferred slip rate of 0.02 mm/yr is calculated from 1 m of vertical displacement in late Pleistocene (ca. 50-100 ka) deposits. The maximum magnitude event for the Sugarloaf fault is considered to be **M** 6.5, the minimum surface faulting magnitude. The Sugarloaf fault is 28 km from Roosevelt and Granite Reef Dams.

Pitaycachi Fault

The most significant earthquake known to have shaken southern Arizona was the 3 May 1887 Sonoran earthquake of maximum intensity MM VIII-IX. The magnitude has been estimated at **M** 7.2 to 7.4 (Herd and McMasters, 1982; Suter, 1999). This earthquake occurred in northern Mexico near the village of Bavispe. Near Phoenix and the region of the damsites, the intensities have been estimated at MM IV-VI.

The source of the 1887 earthquake was the north-south-striking Pitaycachi fault. The event produced 89 km of surface rupture, with down-to-the-west displacement of 0.25 to 4.0 m (Bull and Pearthree, 1988; Suter, 1999). Geomorphological analyses suggest that the prior event to the 1887 rupture occurred 100 to 200 ka. The 9 to 13 m offset of early Pleistocene surfaces suggests an average return period for major surface ruptures (2-3 m) during the Quaternary of as much as 300 to

500 kyr. We adopted a slip rate of 0.1 mm/yr and a maximum earthquake of **M** 7.2 ± 0.3 for this analysis. The closest approach of the Pitaycachi fault to the dams, in this case, Theodore Roosevelt Dam, is about 330 km (Figure 1).

Southern San Andreas Fault

The San Andreas fault accommodates the majority of the motion between the Pacific and North American plates. The fault is marked by fault scarps on Holocene alluvium, right-laterally offset drainages, closed depressions, and shutter ridges. At least one earthquake, a **M** 8 event in 1857, has ruptured the southern half of the fault during historic time. Extensive paleoseismic investigations have revealed a history of surface faulting events along the fault during Holocene time (WGCEP, 1995). Based on differing paleoseismic chronologies, slip rates, slip-per-event, changes in fault geometry, and geomorphic expression, the San Andreas fault has been divided into a number of rupture segments (WGCEP, 1988; 1995). In southern California, these segments include, from north to south, the Cholame, Carrizo, Mojave, San Bernardino Mountains, and Coachella Valley. Although each segment has a distinct paleoseismic history, neighboring segments appear to have ruptured simultaneously in a number of paleoevents. The 1857 earthquake ruptured the Cholame, Carrizo, Mojave, and part of the San Bernardino Mountains segments.

Geologic mapping and seismicity studies indicate that the San Andreas fault is a vertical structure, thus we model the fault dip as 90° ± 10°. We adopt the fault segmentation of WGCEP (1995) and the slip rates and maximum earthquakes assigned in their Southern California earthquake model. The slip rates for individual segments are based on detailed paleoseismic investigations. In addition to rupture of individual segments, we also consider multi-segment rupture, similar to the 'cascade' model of WGCEP (1995), which allows for rupture on contiguous segments (Figure 5). Our multi-segment model allows for a **M** 8 event anywhere on the southern San Andreas fault between Cholame and the southern end of the Salton Trough. The best estimate slip rate is 30 mm/yr, with the range of uncertainty reflecting the maxima and minima calculated from paleoseismic studies on all the fault segments considered (Figure 5).

3.2.2 Background Earthquakes

To account for the hazard from background (floating or random) earthquakes that are not associated with known or mapped faults, a regional seismic source zone was incorporated into the analyses. In most of the western U.S., particularly the Basin and Range Province, the maximum magnitude for earthquakes not associated with known faults usually ranges from **M** 6 to 6½. Repeated events larger than these magnitudes probably produce recognizable fault-or fold-related features at the earth's surface (e.g., Doser, 1985; dePolo, 1994).

Earthquake recurrence estimates in the study region (Figure 1) are required in order to assess the hazard from background earthquakes on the damsites. The historical earthquake catalog developed for the Tucson Terminal Storage Reservoir site (Wong *et al.*, 1995) was utilized and updated using data from the Arizona Earthquake Information Center and the USGS National Earthquake Information Center. This catalog is for the southern Basin and Range Province and its transition zone with the Colorado Plateau (Figure 1). These two areas were combined to insure an adequate number of events in estimating the recurrence.

For most of the events in the catalog, the magnitudes are listed as M_L (local Richter magnitude), M_D (duration magnitude), m_b (body-wave magnitude) values, with a few events having intensity-based M_I values. The M_D, m_b, and M_I were assumed to be equivalent to M_L for this region.

Earthquakes with assigned maximum intensities (I_o) were converted to M_L using the relationship $M_L = 2/3\ I_o + 1$ (Gutenberg and Richter, 1956). All M_L values were assumed to be equivalent to M_w in subsequent calculations.

The updated catalog (1830-1998) contains 304 events. The largest events in the catalog are two M_I 7 earthquakes that occurred in 1830 near San Pedro Valley, Arizona, and 1852 near the northern Colorado River Delta, Mexico (Figure 1). Not much information is known about the 1930 earthquake, including its exact date, magnitude, and location. It is likely to have occurred in the San Pedro Valley region during the 1830's, based on reports from local Native American tribes (DuBois *et al.,* 1982). Based on these and other reports that describe the possibility of surface rupture (now confirmed), DuBois *et al.* (1982) assigned a maximum intensity of modified Mercalli (MM) XI to XII to the event.

No earthquakes of $M_L \geq 5.0$ have occurred in the study region since 1939. Prior to this time, such events have generally occurred in the Yuma County area (Figure 1). Several M_L 4 to 5 earthquakes have occurred in the study region since 1939, including a 1976 M_L 4.9 event in the Prescott region (Figure 1). The largest earthquake in the proximity of the damsites is the 1980 M_I 4.33 event approximately 12 km southwest of Theodore Roosevelt Dam. Other nearby earthquakes include: 1922 M_L 5.0 approximately 20 km southeast of Theodore Roosevelt Dam; 1915 M_L 3.0 approximately 30 km southwest of Granite Reef Diversion Dam; and 1979 M_L 2.5 approximately 6 km southeast of Theodore Roosevelt Dam.

Completeness intervals were estimated for this catalog based on the history of settlement and the seismographic installation and operation in the region. These intervals were used in the evaluation for earthquake recurrence (Figure 6). The recurrence relationship for the study region was estimated using the maximum likelihood procedure developed by Weichert (1980) and the estimated completeness intervals for the region (Figure 6). In the computation of background seismicity recurrence, all events known to be associated with faults considered in the hazard analysis should be removed from the historical catalog. In this case, no such events could be identified and thus no earthquakes were deleted. For the background seismicity, a maximum magnitude of **M** 6.5 ± 0.3 was used.

Dependent events, such as aftershocks, foreshocks, and smaller events within an earthquake swarm, were also identified and removed from the catalogs using the technique developed by Youngs *et al.* (1987). After adjusting the earthquake catalog for dependent events and completeness, 38 events remained in the range **M** 2.5 to 6.5 from which to estimate the recurrence for the study region (Figure 6).

The resulting cumulative mean recurrence relationships, assuming the truncated exponential form of the Gutenberg-Richter relationship of $\log N = a - bM$, are shown in Figure 6. Included are the mean plus and minus one standard deviation curves. Our values are an update of the values calculated by Wong *et al.* (1995) for a similar region (*b*-value of 0.87 and *a*-value of -2.61). A *b*-value of 0.83 and *a*-value of –2.56 were computed by Anderson *et al*. (1986) in a seismotectonic study for Stewart Mountain Dam.

Because of the limited duration and incompleteness of the historical catalog and the small number of events and their narrow magnitude range used in the recurrence calculations, uncertainties in the recurrence parameters for the background seismicity are large. To incorporate these uncertainties into the hazard analysis, we used three *b*-values of 0.7, 0.8, and 0.9 weighted 0.4, 0.4, and 0.2, respectively. An inspection of the resulting recurrence intervals for **M** 5 and 6 events was performed to weight the three *b*-values. The *a*-value of –2.92 was held fixed, since the regressed recurrence curve is well anchored by the seismicity data at small magnitudes.

3.3 GROUND MOTION ATTENUATION

To characterize the attenuation of ground motions in the probabilistic analyses, we have used empirical attenuation relationships appropriate for soft rock sites in the western U.S. Because the damsites are located in an extensional tectonic regime, we have assigned greater weights to the two relationships which are appropriate for regions in the Basin and Range Province. The following relationships were used with their assigned weights (Figure 2): Abrahamson and Silva (1997) with normal faulting factors (0.4); Spudich *et al*. (1999) which was developed from an extensional earthquake strong motion database (0.3); Sadigh *et al*. (1997) (0.15); and Campbell (1997) (0.15). The latter two relationships are based primarily on California strong motion data.

For the southern San Andreas fault, located in the compressional regime of coastal California, four attenuation relationships were used: Abrahamson and Silva (1997), Sadigh *et al.* (1997), Campbell (1997), and Boore *et al.* (1997). They were all equally weighted.

The results of the probabilistic seismic hazard analyses of the dams are presented in terms of ground motion as a function of annual exceedance probability. This probability is the reciprocal of the average return period. Figures 7 and 8 show the mean, median (50th percentile), 5th, 15th, 85th, and 95th percentile hazard curves for peak horizontal acceleration. The 1.0 sec horizontal spectral acceleration hazard is shown on Figures 9 and 10. These fractiles indicate the range of uncertainties about the mean hazard. The uncertainties associated with the background seismicity are contributing to the total uncertainty in the ground motions. At the specified return periods of 10,000 and 50,000 years, the mean horizontal peak and 1.0 sec spectral accelerations are listed on Table 2 for the two dams. The hazard at the two dams is similar because the sources of the hazard for both dams are the same.

The contributions of the various seismic sources to the mean peak horizontal hazard are shown on Figures 11 and 12. Because none of the dams are located near any of the local faults (Figure 3), background earthquakes dominate the high-frequency ground motion hazard (e.g., peak horizontal acceleration). For long-period ground motions, such as 1.0 sec spectral acceleration, the Southern San Andreas fault controls the relatively low long-period hazard at the damsites (Figures 13 and 14).

Figures 15 to 18 illustrate the sensitivity of the mean peak horizontal acceleration and 1.0 sec spectral acceleration hazard to the choice of extensional attenuation relationships. (Note the hazard contribution for the San Andreas fault is not included.) Each hazard curve labeled with one of the four attenuation relationships is calculated using only that relationship. In terms of peak acceleration, the attenuation relationships generally give similar hazard results for all the dams because they do not differ that significantly at low ground motions. The relationship of Spudich *et al.* (1999) gives the lowest peak acceleration hazard (Figures 15 and 16). At 1.0 sec spectral acceleration where the larger magnitude earthquakes are contributing significantly, the differences between attenuation relationships are greater (Figures 17 and 18).

By deaggregating the peak acceleration and 1.0 sec spectral acceleration hazard by magnitude and distance bins, Figures 19 to 26 illustrate the contributions by events. For peak horizontal acceleration at the two return periods of 10,000 and 50,000 years, most of the hazard is derived from **M** 5 to 6.5 background earthquakes at distances of less than 25 km (Figures 19 to 22). For 1.0 sec spectral acceleration, the deaggregated hazard looks significantly different (Figures 23 to 26). As previously discussed, the southern San Andreas fault either dominates or contributes significantly to the long-period hazard. Figures 23 to 26 illustrate dramatically the **M** 7 to 8 contributions beyond distances of 250 km. Table 3 lists the mean magnitude ($\overline{M}$), distance ($\overline{D}$), and epsilon ($\overline{\varepsilon}$) of the distributions. Epsilon is the difference between the logarithm of the ground motion amplitude and the mean logarithm of ground motion measured in units of the standard deviation (σ) of the logarithm of the ground motion.

Abrahamson, N.A. and Silva, W.J., 1997, Empirical response spectral attenuation relations for shallow crustal earthquakes: Seismological Research Letters, v. 68, p. 94-127.

Aki, K., 1983, Seismological evidence in support of the existence of "Characteristic Earthquakes": Earthquake Notes, v. 54, p. 60-61.

Anderson, J.G., 1979, Estimating the seismicity from geological structure for seismic risk studies: Bulletin of the Seismological Society of America, v. 69, p. 135-158.

Anderson, L.W., Piety, L.A., and LaForge, R.C., 1987, Seismotectonic investigations, Theodore Roosevelt Dam, Salt River Project, Arizona: U. S. Bureau of Reclamation Seismotectonic Report 87-5, 46 p.

Anderson, L.W., Piety, L.A., and Hansen, R.A., 1986, Seismotectonic investigations, Stewart Mountain Dam, Salt River Project, Arizona: U. S. Bureau of Reclamation Seismotectonic Report 86-2, 41 p.

Bausch and Brumbaugh, 1997, Relocation study of early Arizona earthquakes: Events of 1906, 1910, and 1912: unpublished report prepared for Arizona Division of Emergency Management, Earthquake Program, 65 p. + Appendices.

Boore, D.M., Joyner, W.B., and Fumal, T.E., 1997, Equations for estimating horizontal response spectra and peak acceleration from western North American earthquakes: A summary of recent work: Seismological Research Letters, v. 68, p. 128-153.

Brumbaugh, D. S., 1987, A tectonic boundary for the Southern Colorado Plateau: Tectonophysics, v. 136, p. 125-136.

Bull, W. B. and Pearthree, P.A., 1988, Frequency and size of Quaternary surface ruptures of the Pitaycachi fault, northeastern Sonora, Mexico: Bulletin of the Seismological Society of America, v. 78, p. 956-978.

Campbell, K.W., 1997, Empirical near-source attenuation relationships for horizontal and vertical components of peak ground acceleration, peak ground velocity, and pseudo-absolute acceleration response spectra: Seismological Research Letters, v. 68, p. 154-179.

Cornell, C.A., 1968, Engineering seismic risk analysis: Bulletin of the Seismological Society of America, v. 58, p. 1583-1606.

dePolo, C.M., 1994, The maximum background earthquake for the Basin and Range Province, western North America: Bulletin of the Seismological Society of America, v. 84, p. 466-472.

Doser, D.I., 1985, The 1983 Borah Peak, Idaho and 1959 Hebgen Lake, Montana earthquakes—Models for normal fault earthquakes in the Intermountain seismic belt, *in* R.S. Stein and R.C. Bucknam (eds.), Proceedings of Workshop XXVIII on the Borah Peak, Idaho, Earthquake: U.S. Geological Survey Open-File Report 85-290, p. 368-384.

Doser, D.I. and Smith, R.B., 1989, An assessment of source parameters of earthquakes in the Cordillera of the western United States: Bulletin of the Seismological Society of America, v. 79, p. 1383-1409.

DuBois, S.M., Smith, A.W., Nye, N.K., and Nowak, T.A., 1982, Arizona earthquakes, 1776-1980: Arizona Bureau of Geology and Mineral Technology Bulletin 192, 456 p.

Ertec Western, 1981, Seismotectonic Study, New Waddell Damsite, Arizona: unpublished report prepared for U.S. Bureau of Reclamation, 32 p.

Gutenberg, B. and Richter, C.F., 1956, Earthquake magnitude, intensity, energy and acceleration: Bulletin of the Seismological Society of America, v. 46, p. 105-145.

Hanks, T.C. and Kanamori, H. 1979, A moment magnitude scale: Journal of Geophysical Research, v. 84, p. 2348-2350.

Herd, D. G. and McMasters, C. R., 1982, Surface faulting in the Sonora, Mexico, earthquake of 1887: Abstracts with Programs, Geological Society of America v. 14, p. 172.

McGuire, R.K., 1974, Seismic structural response risk analysis incorporating peak response regressions on earthquake magnitude and distance: Massachusetts Institute of Technology Department of Civil Engineering/Research Report R74-51.

McGuire, R.K., 1978, FRISK: Computer program for seismic risk analysis using faults as earthquake sources: U.S. Geological Survey Open-File Report 78-1007.

Menges, C.M. and McFadden, L.D., 1981, Evidence for the latest-Miocene to Pliocene transition from Basin-Range tectonic to post-tectonic landscape evolution in southeastern Arizona: Arizona Geological Society Digest, v. 13, p. 151-160.

Molnar, P., 1979, Earthquake recurrence intervals and plate tectonics: Bulletin of the Seismological Society of America, v. 69, p. 115-133.

Morgan, P. and Swanberg, C.A., 1985, on the Cenozoic uplift and tectonic stability of the Colorado Plateau: Journal of Geodynamics, v. 3, p. 39-63.

Pearthree, P. A., 1998, Quaternary fault data and map of Arizona: Arizona Geological Survey Open-File Report 98-24, 122 p.

Pearthree, P. A., Vincent, K. R., Brazier, R., Fellows, L.D., and Davis, O.K., 1995, Seismic hazard posed b y the Sugarloaf fault, central Arizona: Arizona Geological Survey Open-File Report 95-7, 41, p.

Piety, L.A. and Anderson, L.W., 1990, Seismotectonic investigation for Horseshoe and Bartlett Dams – Salt River Project, Arizona: U. S. Bureau of Reclamation Seismotectonic Report 90-7, 59 p.

Piety, L.A. and Anderson, L. W. 1991, The Horseshoe fault: evidence for prehistoric surface-rupturing earthquakes in central Arizona: Arizona Geology, v. 21, p. 1-8.

Sadigh, K., Chang, C.Y., Egan, J.A., Makdisi, F., and Youngs, R.R., 1997, Attenuation relationships for shallow crustal earthquakes based on California strong motion data: Seismological Research Letters, v. 68, p. 180-189.

Schwartz, D.P. and Coppersmith, K.J., 1984, Fault behavior and characteristic earthquakes--examples from the Wasatch and San Andreas fault zones: Journal of Geophysical Research, v. 89, p. 5681-5698.

Skotnicki, S.J., Leighty, R.S., and Pearthree, P.A., 1997, Geologic map of the Wildcat Hill quadrangle, Maricopa County, Arizona: Arizona Geological Survey Open-File Report 97-2, 17 p., scale 1:24,000.

Spudich, P., Joyner, W.B., Lindh, A.G., Boore, D.M., Margaris, B.M., and Fletcher, J.B., 1999, SEA99 - A revised ground motion prediction relation for use in extensional tectonic regimes: Bulletin of the Seismological Society of America, v. 89, p. 1156-1170.

Suter, M., 1999, Surface rupture of the 3 May 1887 M_W 7.4 Sonora, Mexico, earthquake and structure of the underlying Basin and Range faults (abs.): Abstract with Programs, Geological Society of America, v. 31, p. 128.

Weichert, D.H., 1980, Estimation of the earthquake recurrence parameters for unequal observation periods for different magnitudes: Bulletin of the Seismological Society of America, v. 70, p. 1337-1346.

Wells, D. L. and Coppersmith, K. J., 1994, New empirical relationships among magnitude, rupture length, rupture width, rupture area, and surface displacement: Bulletin of the Seismological Society of America, v. 84, p. 974-1002.

Wesnousky, S.G., 1986, Earthquakes, Quaternary faults, and seismic hazard in California: Journal Geophysical Research, v. 91, p. 12,587-12,631.WGCEP, 1995, Seismic hazrds in southern California: Probable earthquakes, 1994 to 2024: Bulletin of the Seismological Society of America, v. 85, p. 379-439.

Wong, I.G., Bott, J.D.J., Fenton, C. H., Silva, W.J., and Li, S., 1995, Seismicity and earthquake ground motion evaluation, Tucson Terminal Storage Reservoir Site, Central Arizona Project: unpublished report prepared for U. S. Bureau of Reclamation by Woodward-Clyde Federal Services.

Wong, I.G., Dober, M., and Fenton, C.H., 2000, Probabilistic seismic hazard analyses, Bartlett, Horseshoe, Stewart Mountain, and New Waddell Dams, Southern Arizona: unpublished report prepared for U.S. Bureau of Reclamation by URS Greiner Woodward-Clyde Federal Services.

Wong, I.G. and Humphrey, J.R., 1989, Contemporary seismicity, faulting, and the state of stress in the Colorado Plateau: Geological Society of America Bulletin, v. 101, p. 1127-1146.

Working Group on California Earthquake Probabilities, 1988, Probabilities of large earthquakes occurring in California on the San Andreas fault: U.S. Geological Survey Open-File Report 88-398, 62 p.

Working Group for California Earthquake Probabilities, 1995, Seismic hazards in southern California: Probable earthquakes, 1994 to 2024: Bulletin of the Seismological Society of America, v. 85, p. 379-439.

Youngs, R.R. and Coppersmith, K.J., 1985, Implications of fault slip rates and earthquake recurrence models to probabilistic seismic hazard estimates: Bulletin of the Seismological Society of America, v. 75, p. 939-964.

Youngs, R.R., Swan, F.H., Power, M.S., Schwartz, D.P., and Green, R.K., 1987, Probabilistic analysis of earthquake ground shaking hazard along the Wasatch Front, Utah, *in* P.L. Gori and W.W. Hays (eds.), Assessment of Regional Earthquake Hazards and Risk Along the Wasatch Front, Utah: U.S. Geological Survey Open-File Report 87-585, v. 2, p. M1-M110.

TABLE 1 FAULT SOURCE PARAMETERS

Map Source	Fault Name	Maximum Rupture Length (km)	Maximum Magnitude (M)	Dip (º)	Approximate Age	Probability of Activity	Slip Rate (mmyr^{-1})	Comments
Skotnicki *et al.* (1997)	Carefree Fault Zone	11	6.2 (0.3) 6.5 (0.4) 6.8 (0.3)	45º SW (0.1) 60º SW (0.6) 80º SW (0.3)	Middle to Late Pleistocene (<750 ka)	0.7	0.001 (0.3) 0.03 (0.4) 0.2 (0.3)	Slip rate based on 3 m vertical topographic offset. Late Pleistocene and Holocene deposits are not offset (Pearthree, 1998). Pearthree (1998) states that the fault dip is "high angle". Maximum magnitude from minimum earthquake required to cause surface rupturing in the Basin and Range.
Piety and Anderson (1990, 1991)	Horseshoe Fault Unsegmented (0.6) Segmented (0.4): Hell Canyon (0.5) Reservoir (0.5)	 23 14 9	 6.3 (0.3) 6.6 (0.4) 6.9 (0.3) 6.2 (0.3) 6.5 (0.4) 6.8 (0.3) 6.2 (0.3) 6.5 (0.4) 6.8 (0.3)	Hell Canyon section: 45º E (0.3) 60º E (0.4) 75º E (0.3) Reservoir Section: 55º NE (0.3) 70º NE (0.4) 85º NE (0.3)	Holocene (<15 ka)	1.0	0.001 (0.3) 0.03 (0.4) 0.2 (0.3)	Slip rate is based on no more than 5 m of vertical displacement on the Hell Canyon section in the past 150 ky, and no more than 2 m vertical displacement on the Horseshoe Reservoir section in the past 200 to 300 kyr (Pearthree 1998). Dip of the Hell Canyon section of the fault is not recorded (Pearthree, 1998); therefore the fault dip for this section of the fault is based on averages for Basin and Range normal faults. Fault dip for reservoir section is taken from Piety and Anderson (1990, 1991)
Bull and Pearthree (1988); Suter (1999)	Pitaycachi Fault	89	6.9 (0.3) 7.2 (0.4) 7.5 (0.3)	45□ W (0.3) 60□ W (0.4) 75□ W(0.3)	Historic (1887)	1.0	0.1 (1.0)	A M 7.2 to 7.4 earthquake in 1887 produced 89 km of surface rupture, with up to 4.0 m of normal, down-to-the-west displacement (Bull & Pearthree, 1988). Slip rate is an upper bound estimate based on displacement data of Suter (1999).
Ertec (1981); Anderson *et al*. (1986)	Sugarloaf Fault	8	6.2 (0.3) 6.5 (0.4) 6.8 (0.3)	60º W (0.3) 75º W (0.4) 90º W (0.3)	Late to latest Pleistocene (< 130 ka)	1.0	0.005 (0.2) 0.02 (0.6) 0.2 (0.2)	Trench exposures show offsets of upper and uppermost Pleistocene deposits. middle and late Holocene deposits are not faulted. Slip rate based on no more than 1 m vertical displacement in the past 50 - 100 kyr. Maximum earthquake based on minimum magnitude for surface rupture in the Basin and Range. Maximum rupture length and dip from Pearthree (1998)

Table 2
Mean Probabilistic Peak Horizontal and 1.0 sec Spectral Accelerations

	PGA (g)		1 sec SA (g)	
	10,000 yr	**50,000 yr**	**10,000 yr**	**50,000 yr**
Granite Reef Diversion Dam	0.15	0.27	0.15	0.23
Theodore Roosevelt Dam	0.14	0.27	0.14	0.22

Table 2
Earthquake Catalog Completeness Intervals and Number of Events Used in Recurrence Calculations

Magnitude Range	Time Period	Number of Events
3.0 – 3.5	1981 – Present	
3.5 – 4.0	1970 – Present	
4.0 – 4.5	1962 – Present	
4.5 – 5.0	1940 – Present	
5.0 – 5.5	1900 – Present	
5.5 – 6.0	1880 – Present	

Table 3
$\overline{M}$, $\overline{D}$, and $\overline{\varepsilon}$

Granite Reef Diversion Dam

	PGA		1 sec	
	10,000 yrs	**50,000 yrs**	**10,000 yrs**	**50,000 yrs**
$\overline{M}$	5.9	5.9	6.7	6.7
$\overline{D}$	18.4	12.5	144.2	108.4
$\overline{\varepsilon}$	0.57	0.95	1.20	1.45

Theodore Roosevelt Dam

	PGA		1 sec	
	10,000 yrs	**50,000 yrs**	**10,000 yrs**	**50,000 yrs**
$\overline{M}$	5.8	5.8	6.7	6.6
$\overline{D}$	18.1	12.0	159.7	118.3
$\overline{\varepsilon}$	0.48	0.89	1.15	1.38

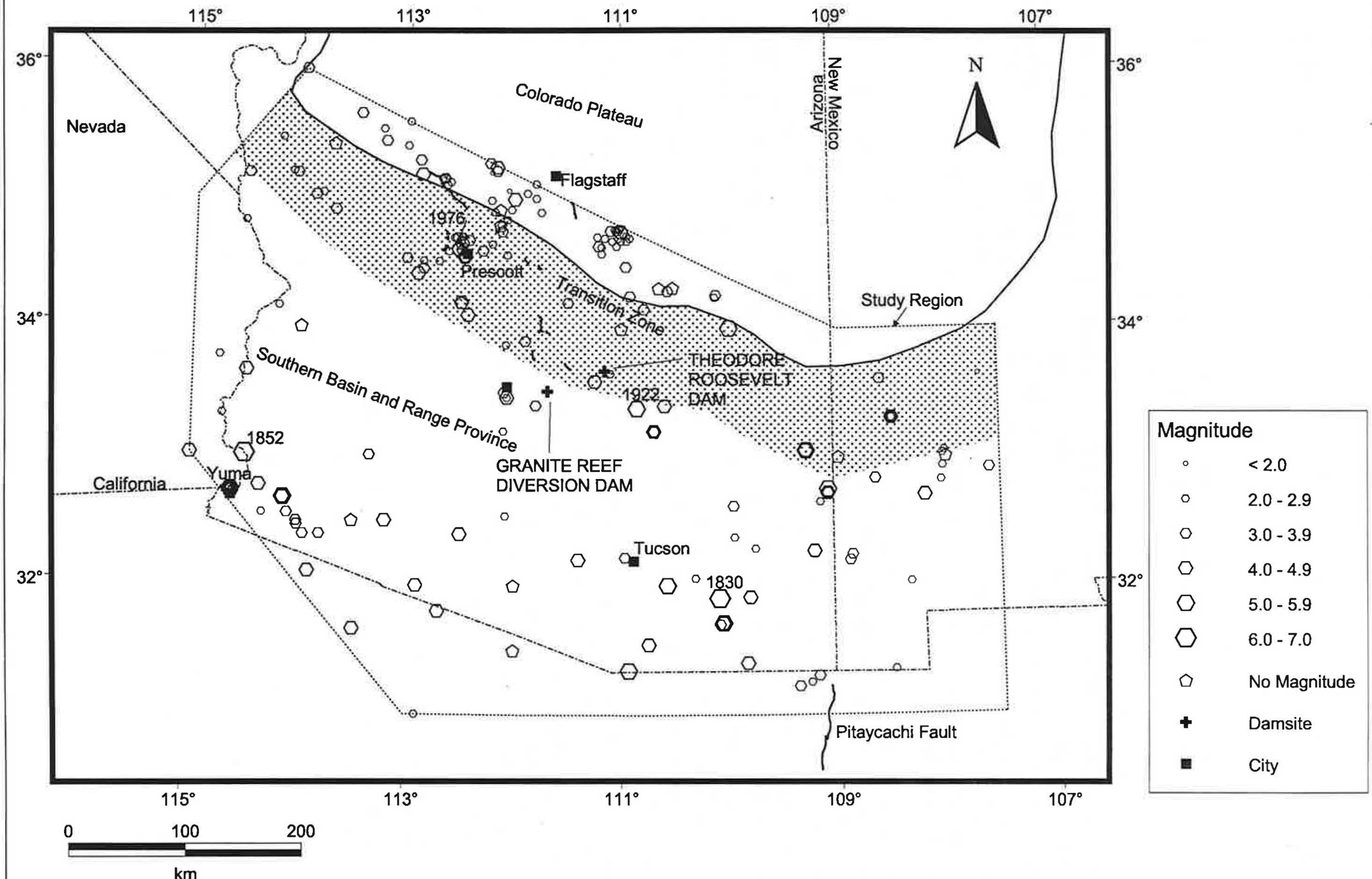

URS	Project No. 68-FUSBR232.00	HISTORICAL SEISMICITY OF THE STUDY REGION, 1830 TO 1998	Figure 1
	Roosevelt and Granite Reef Dams		

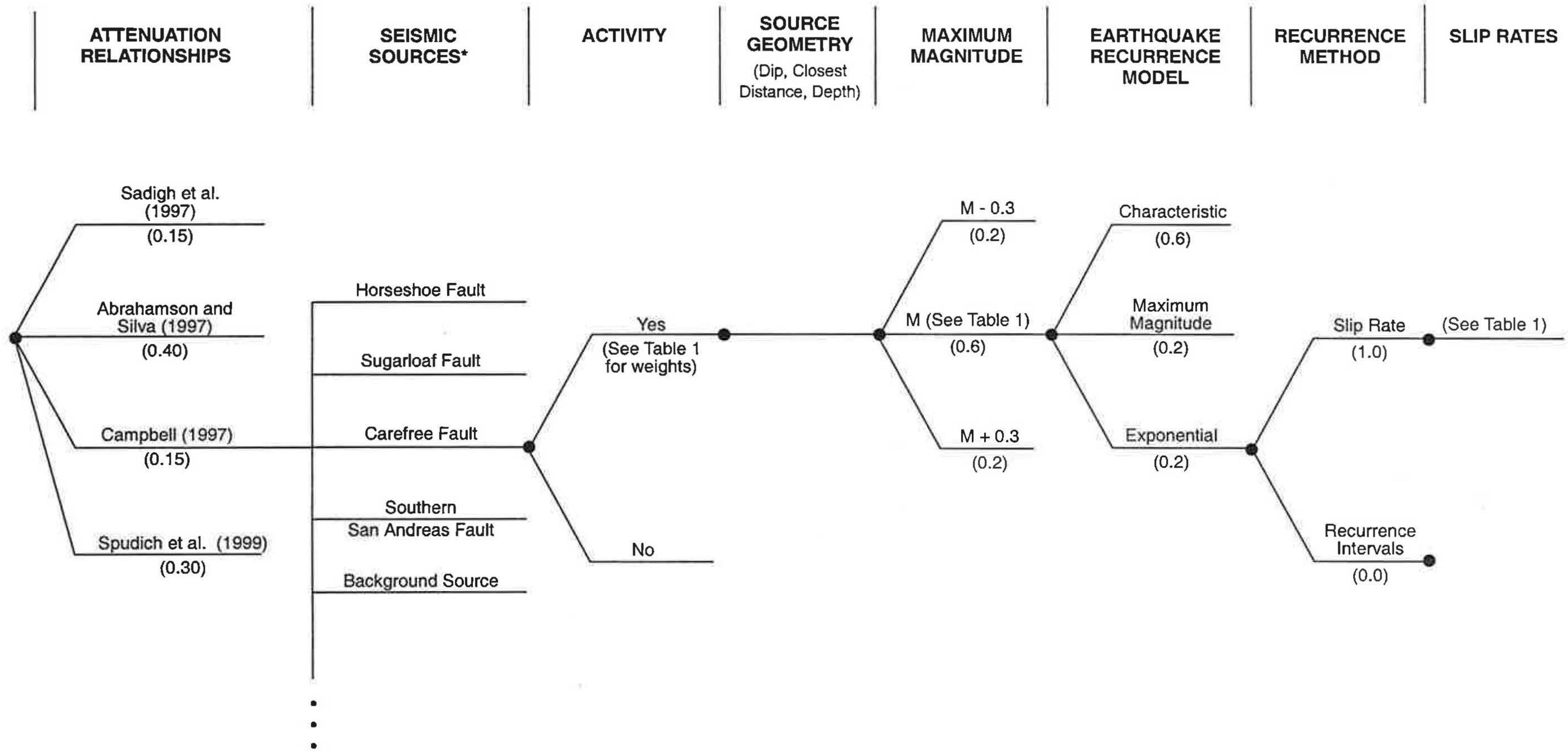

URS	Project No. 68-FUSBR207.00 Roosevelt and Granite Reef Dams	SEISMIC HAZARD MODEL LOGIC TREE	Figure 2

68-FUSBR207.00-00000/122302/gos

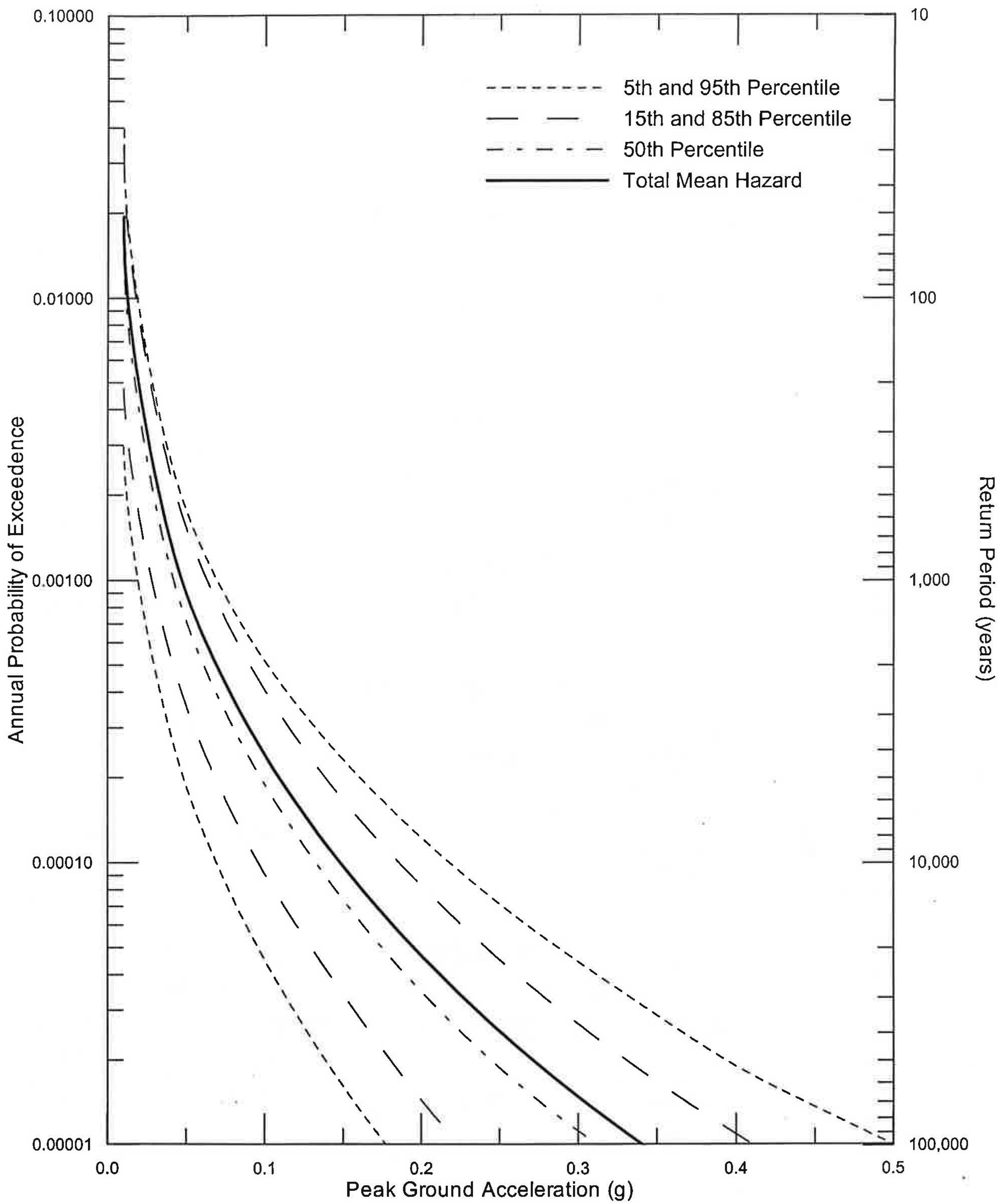

URS	Project No. 68-FUSBR207.00 Roosevelt and Granite Reef Dams	SEISMIC HAZARD CURVES FOR MEAN PEAK HORIZONTAL ACCELERATION FOR GRANITE REEF DAM	Figure 7

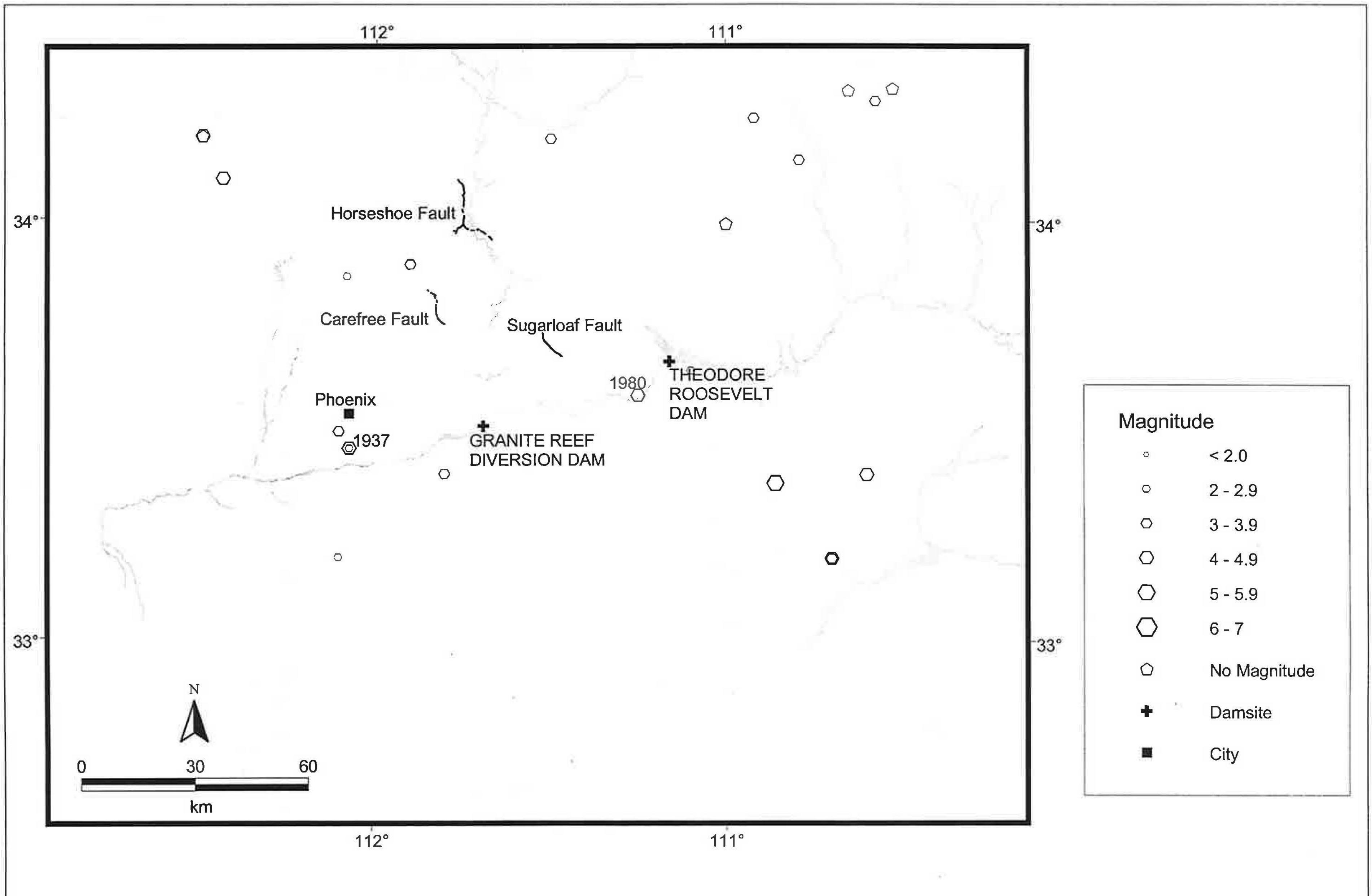

URS	Project No. 68-FUSBR232.00 Roosevelt and Granite Reef Dams	QUATERNARY FAULT SOURCES INCLUDED IN THE HAZARD ANALYSIS	Figure 3

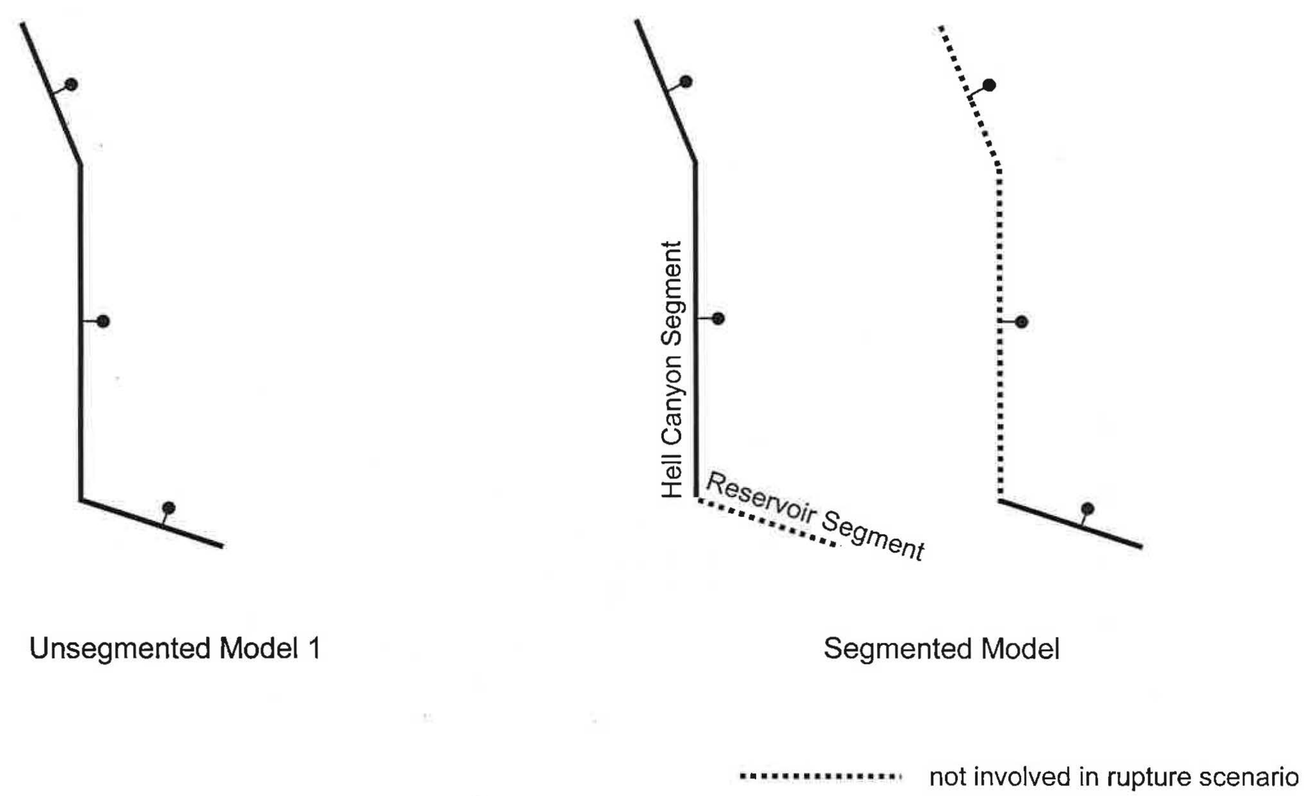

URS	Project No. 68-FUSBR207.00	RUPTURE SCENARIOS OF THE HORSESHOE FAULT	Figure 4
	Roosevelt and Granite Reef Dams		

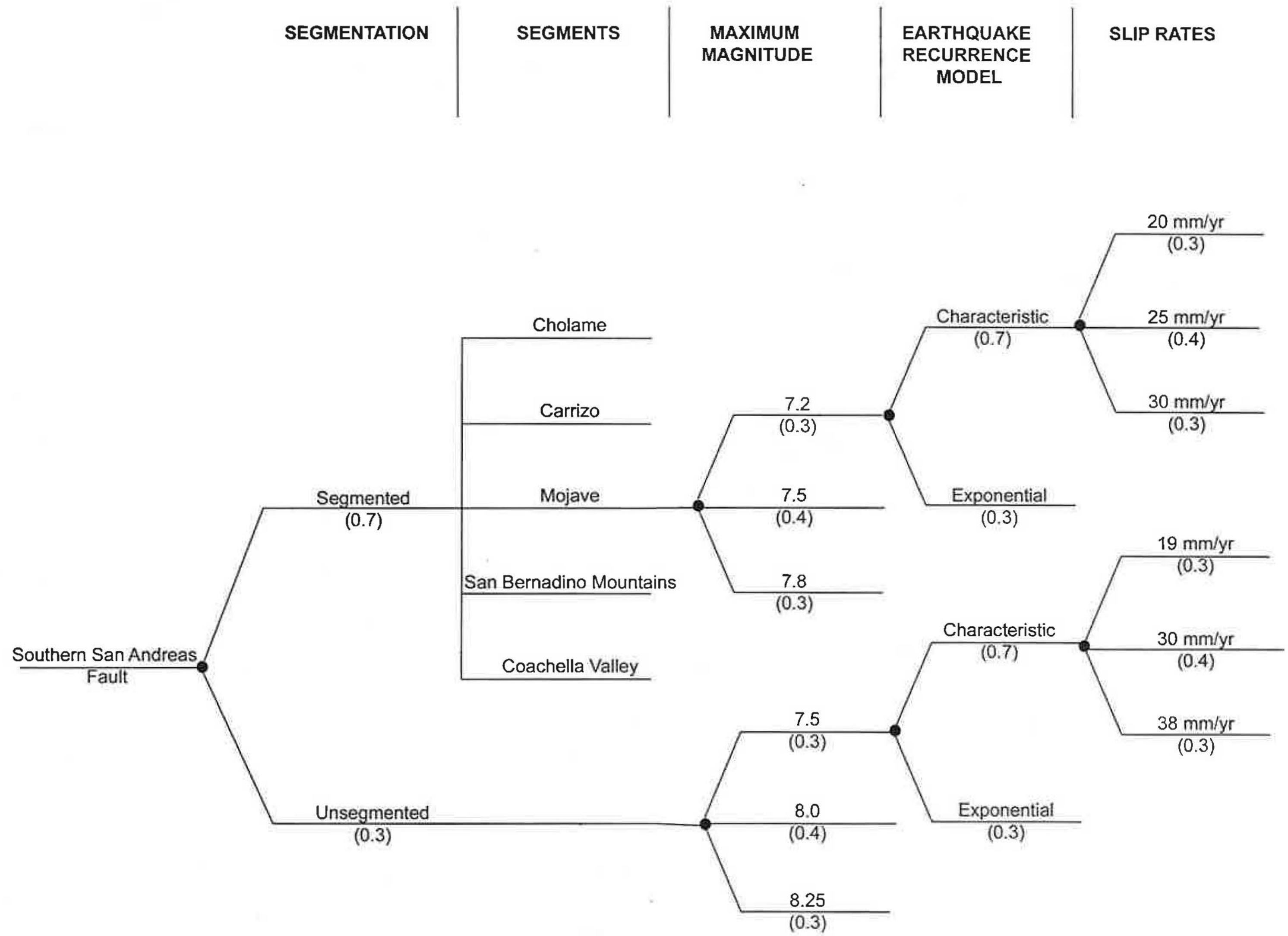

URS	Project No. 68-FUSBR207.00 Roosevelt and Granite Reef Dams	LOGIC TREE FOR SOUTHERN SAN ANDREAS FAULT	Figure 5

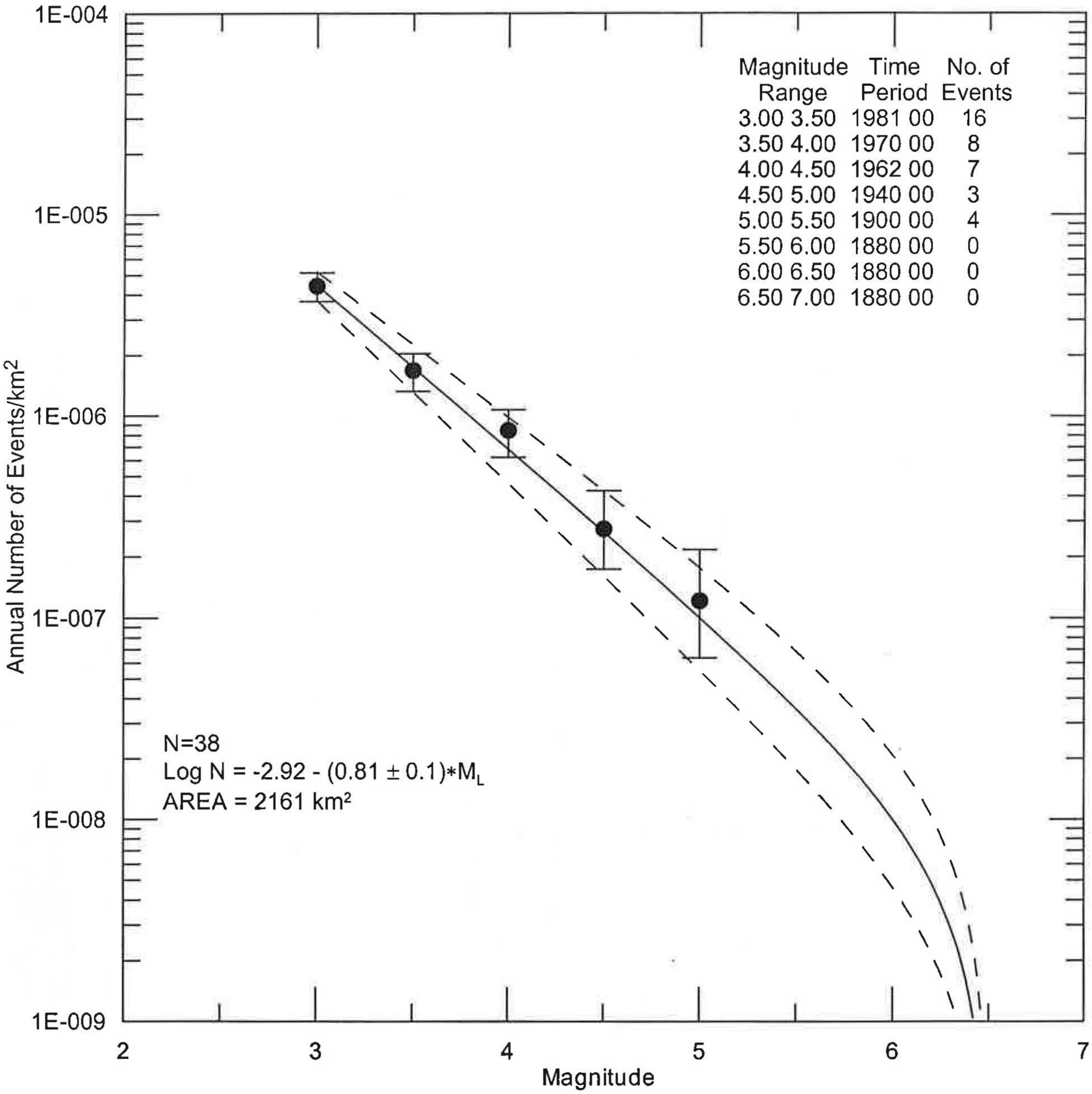

URS	Project No. 68-FUSBR232.00 Roosevelt and Granite Reef Dams	EARTHQUAKE RECURRENCE OF THE STUDY REGION	Figure 6

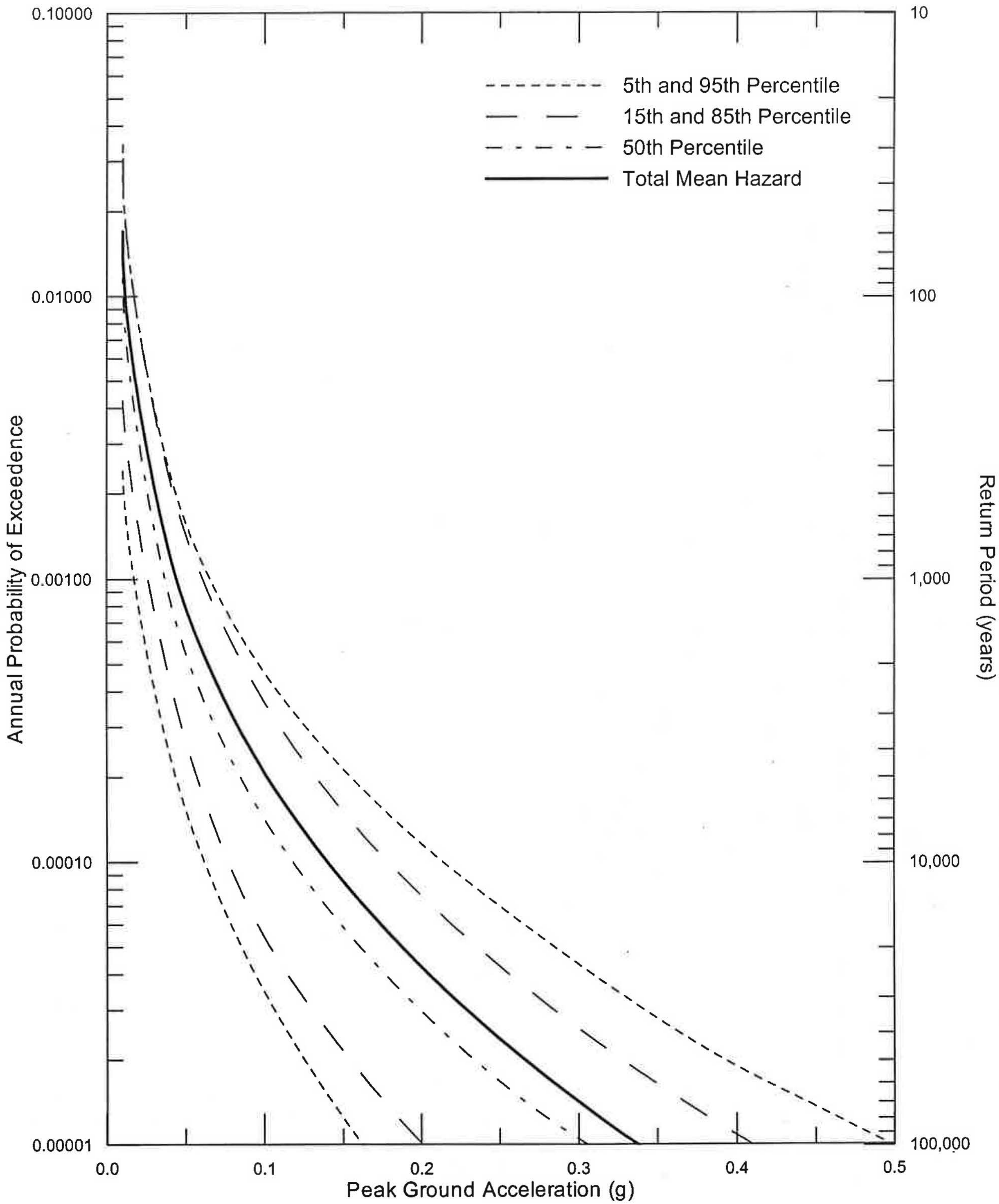

URS	Project No. 68-FUSBR207.00 Roosevelt and Granite Reef Dams	SEISMIC HAZARD CURVES FOR MEAN PEAK HORIZONTAL ACCELERATION FOR THEODORE ROOSEVELT DAM	Figure 8

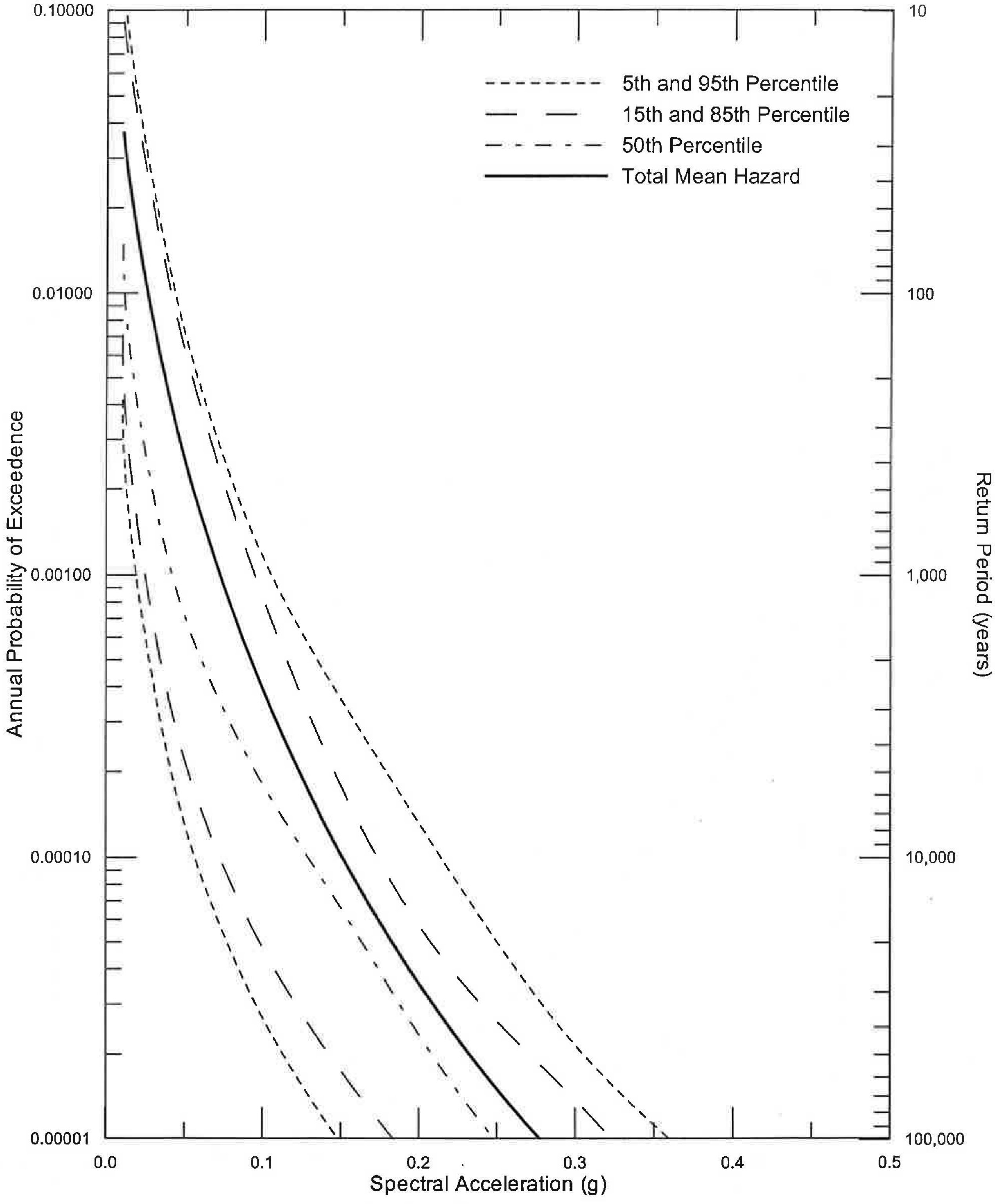

URS	Project No. 68-FUSBR207.00 Roosevelt and Granite Reef Dams	SEISMIC HAZARD CURVES FOR MEAN 1.0 SEC SPECTRAL ACCELERATION FOR GRANITE REEF DAM	Figure 9

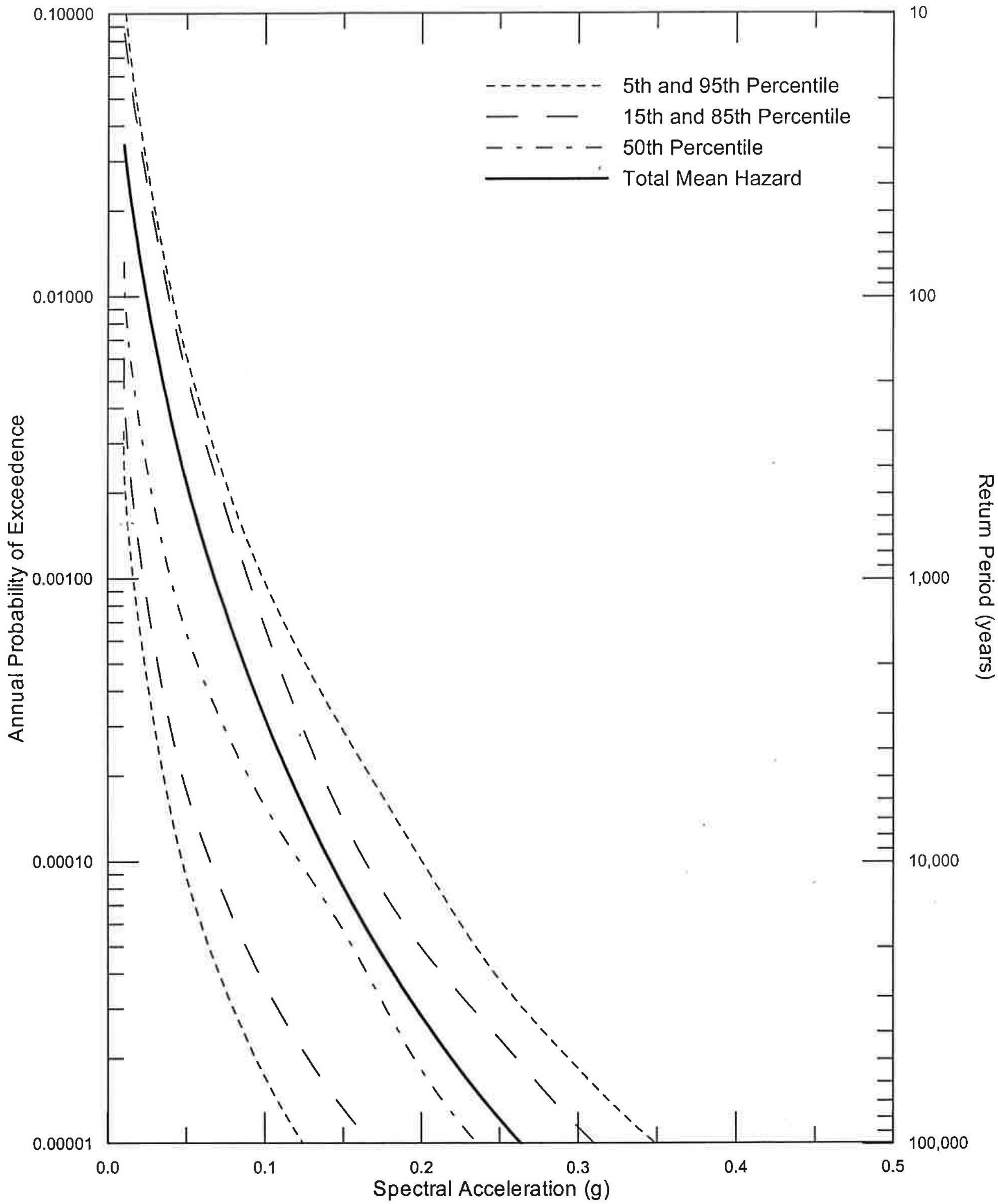

URS	Project No. 68-FUSBR207.00 Roosevelt and Granite Reef Dams	SEISMIC HAZARD CURVES FOR MEAN 1.0 SEC SPECTRAL ACCELERATION FOR THEODORE ROOSEVELT DAM	Figure 10

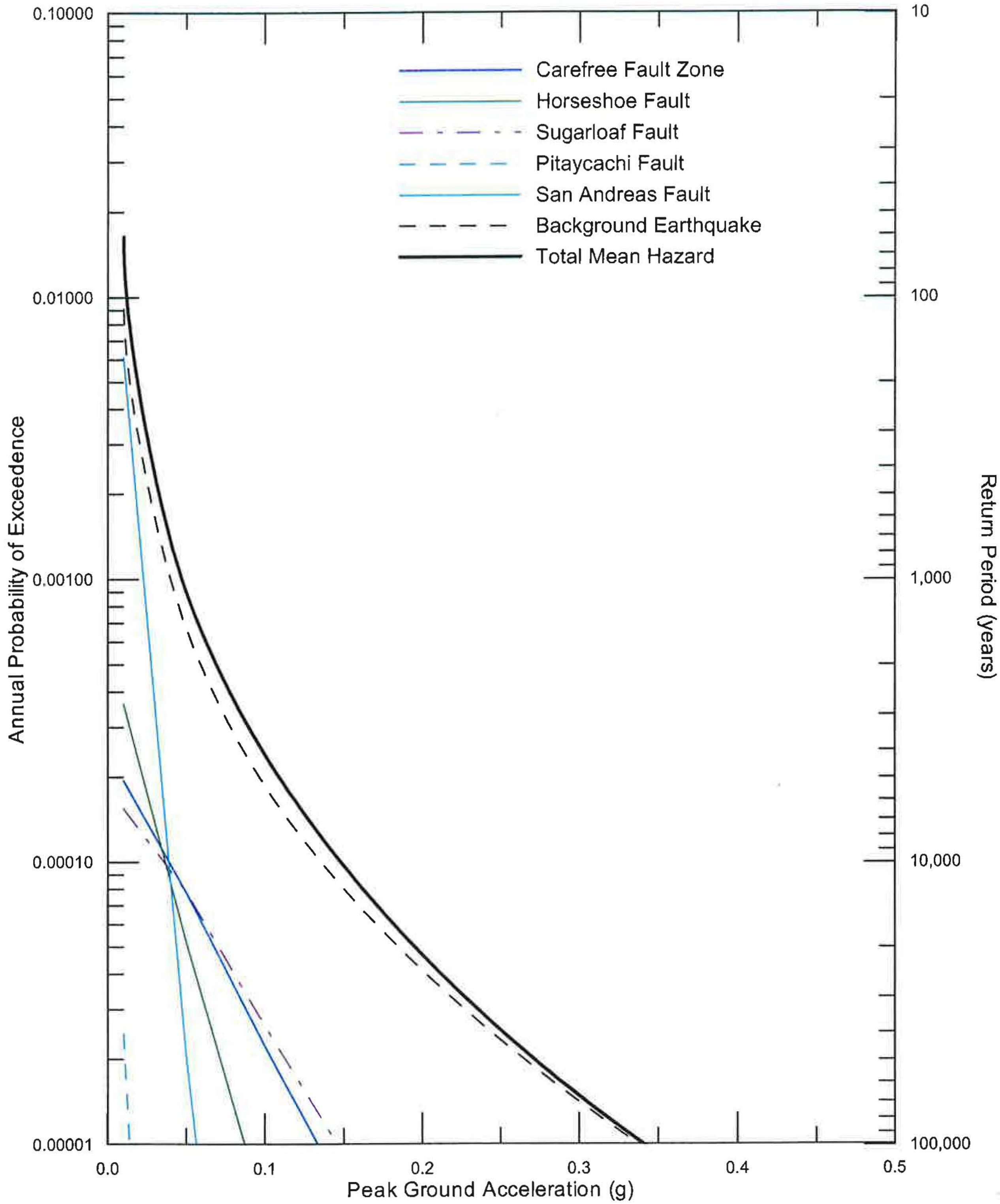

URS	Project No. 68-FUSBR207.00 Roosevelt and Granite Reef Dams	SEISMIC SOURCE CONTRIBUTIONS TO MEAN PEAK HORIZONTAL ACCELERATION HAZARD FOR GRANITE REEF DAM	Figure 11

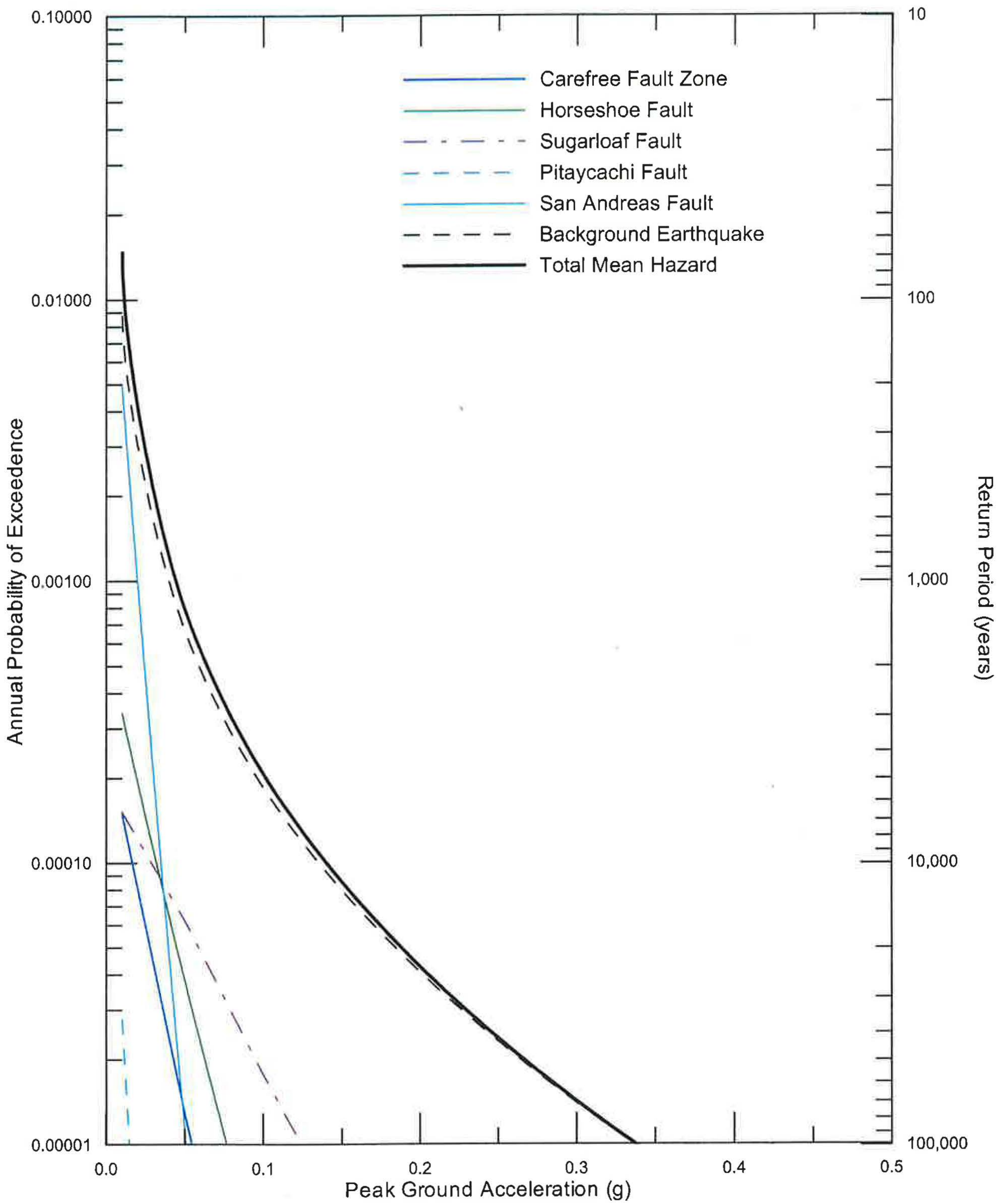

URS	Project No. 68-FUSBR207.00 Roosevelt and Granite Reef Dams	SEISMIC SOURCE CONTRIBUTIONS TO MEAN PEAK HORIZONTAL ACCELERATION HAZARD FOR THEODORE ROOSEVELT DAM	Figure 12

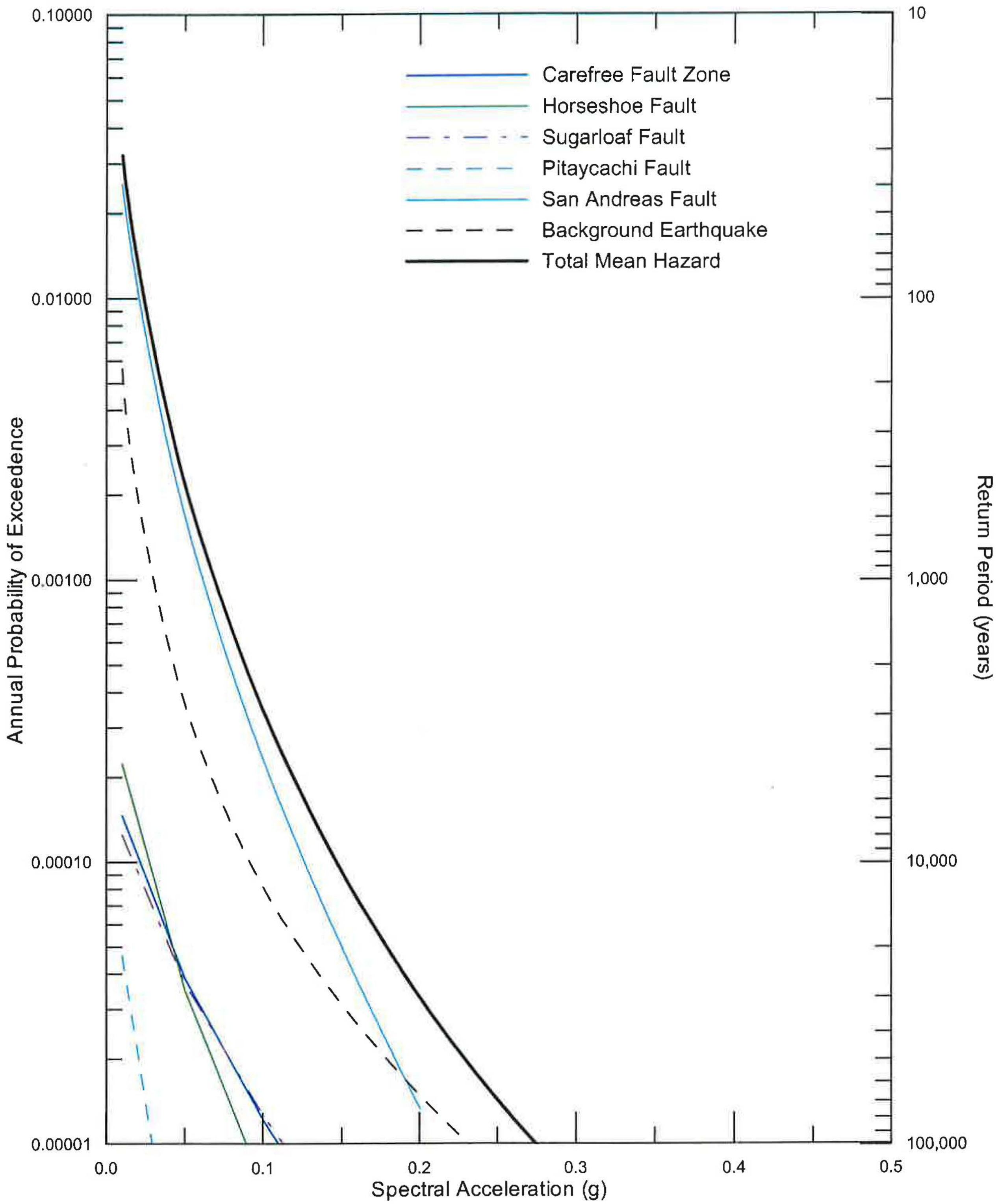

URS	Project No. 68-FUSBR207.00 Roosevelt and Granite Reef Dams	SEISMIC SOURCE CONTRIBUTIONS TO MEAN 1.0 SEC SPECTRAL ACCELERATION HAZARD FOR GRANITE REEF DAM	Figure 13

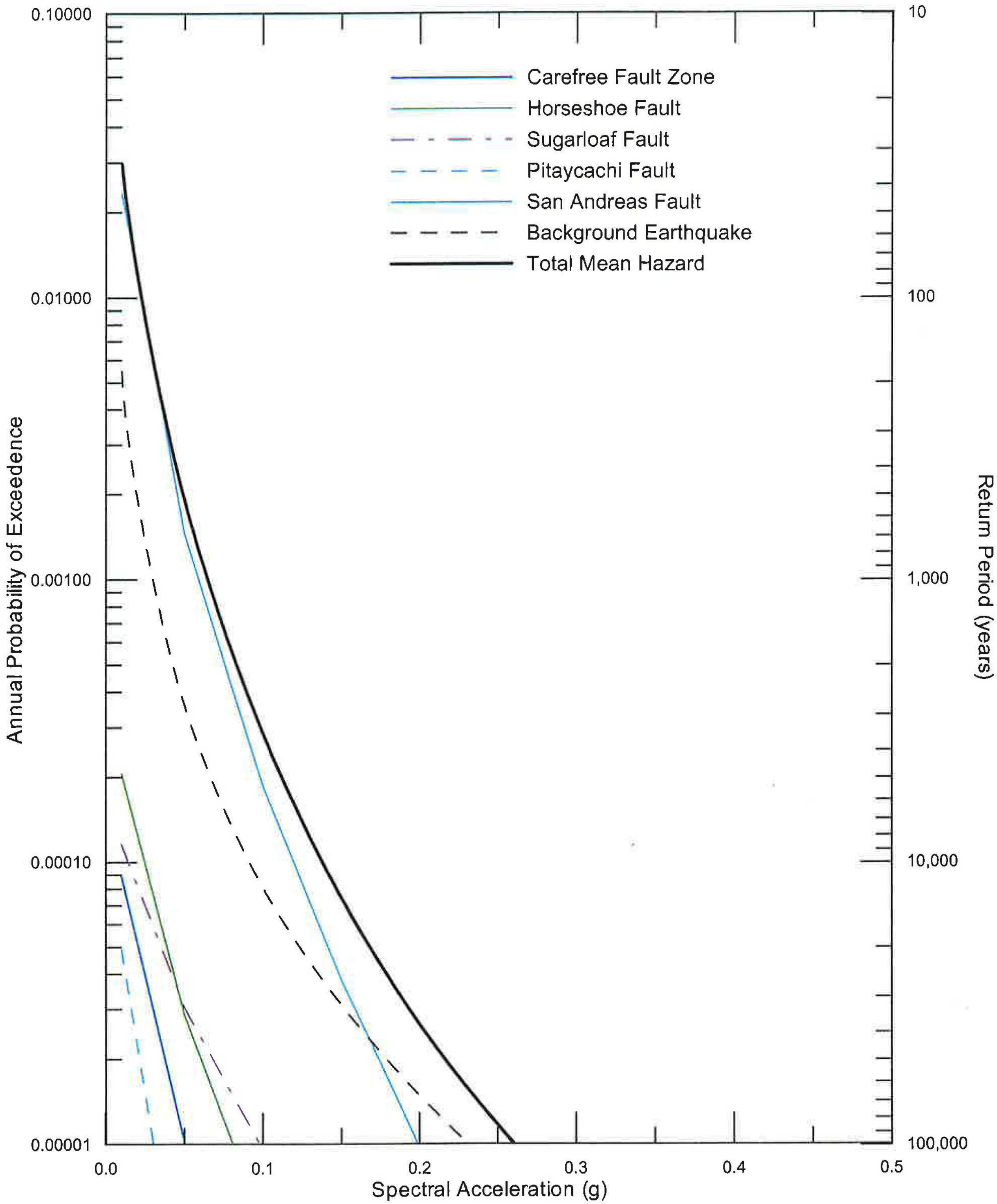

URS	Project No. 68-FUSBR207.00 Roosevelt and Granite Reef Dams	SEISMIC SOURCE CONTRIBUTIONS TO MEAN 1.0 SEC SPECTRAL ACCELERATION HAZARD FOR THEODORE ROOSEVELT DAM	Figure 14

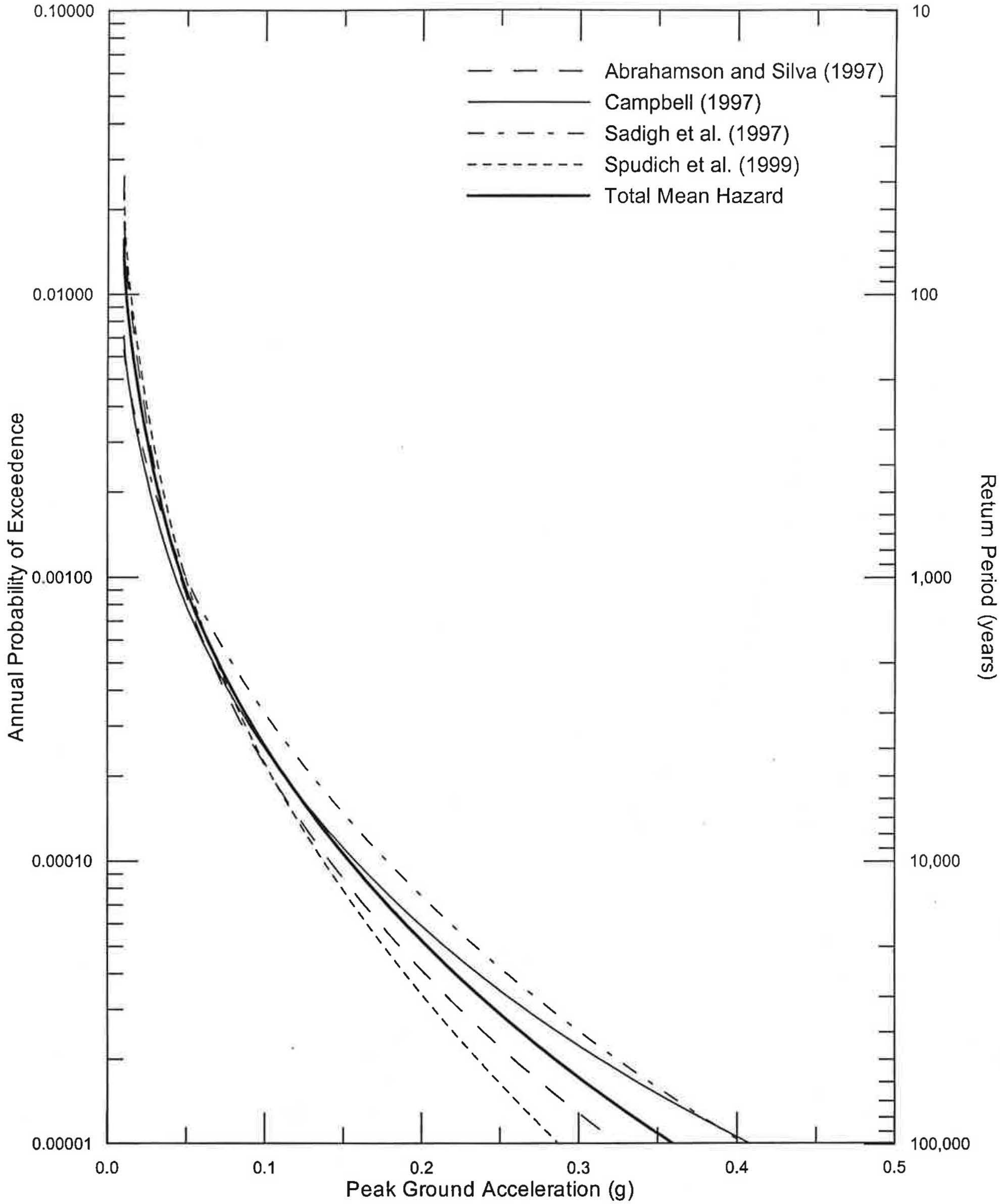

URS	Project No. 68-FUSBR207.00	MEAN PEAK HORIZONTAL ACCELERATION HAZARD: SENSITIVITY TO ATTENUATION RELATIONS FOR GRANITE REEF DAM	Figure 15
	Roosevelt and Granite Reef Dams		

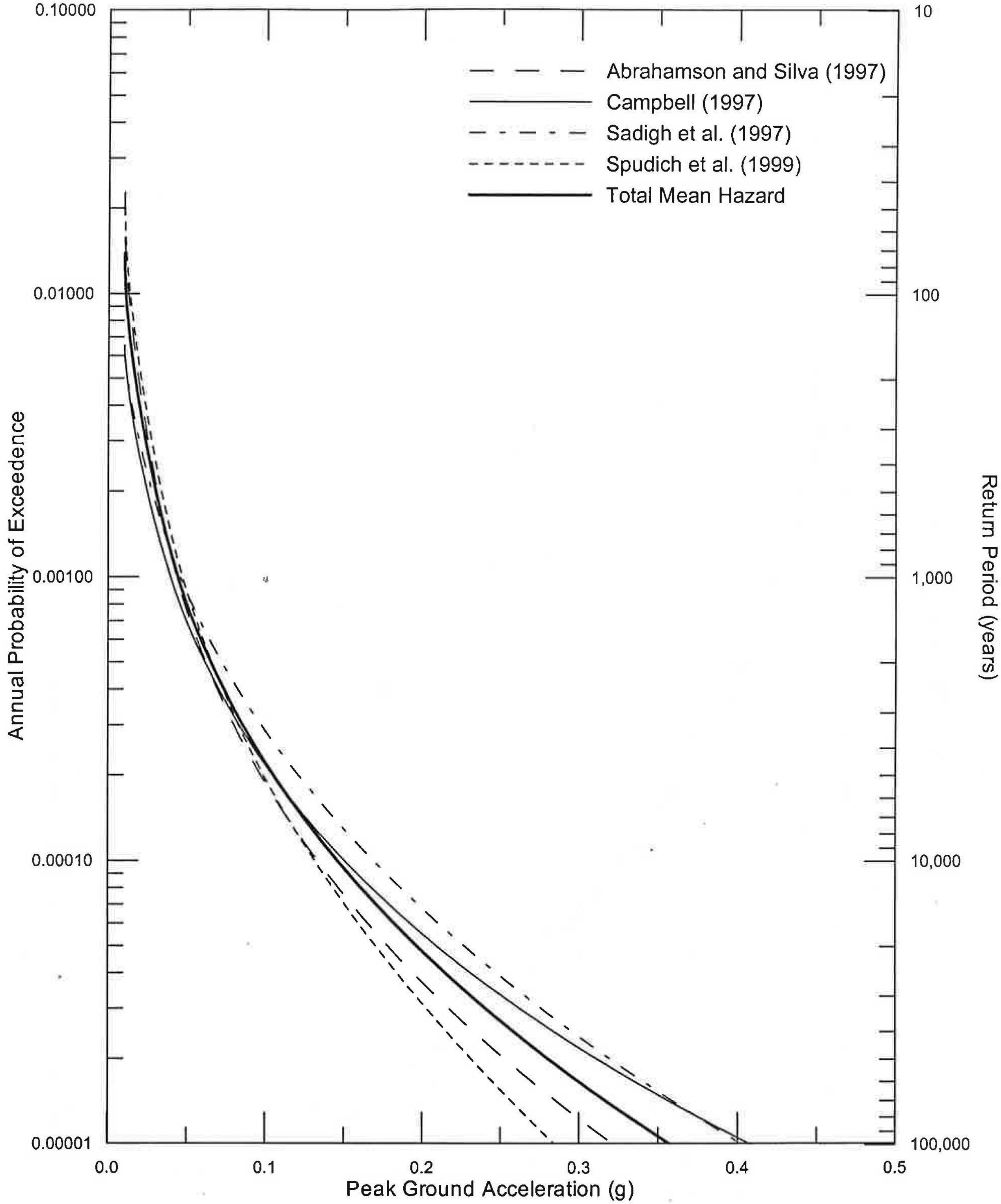

URS	Project No. 68-FUSBR207.00	MEAN PEAK HORIZONTAL ACCELERATION HAZARD: SENSITIVITY TO ATTENUATION RELATIONS FOR THEODORE ROOSEVELT DAM	Figure 16
	Roosevelt and Granite Reef Dams		

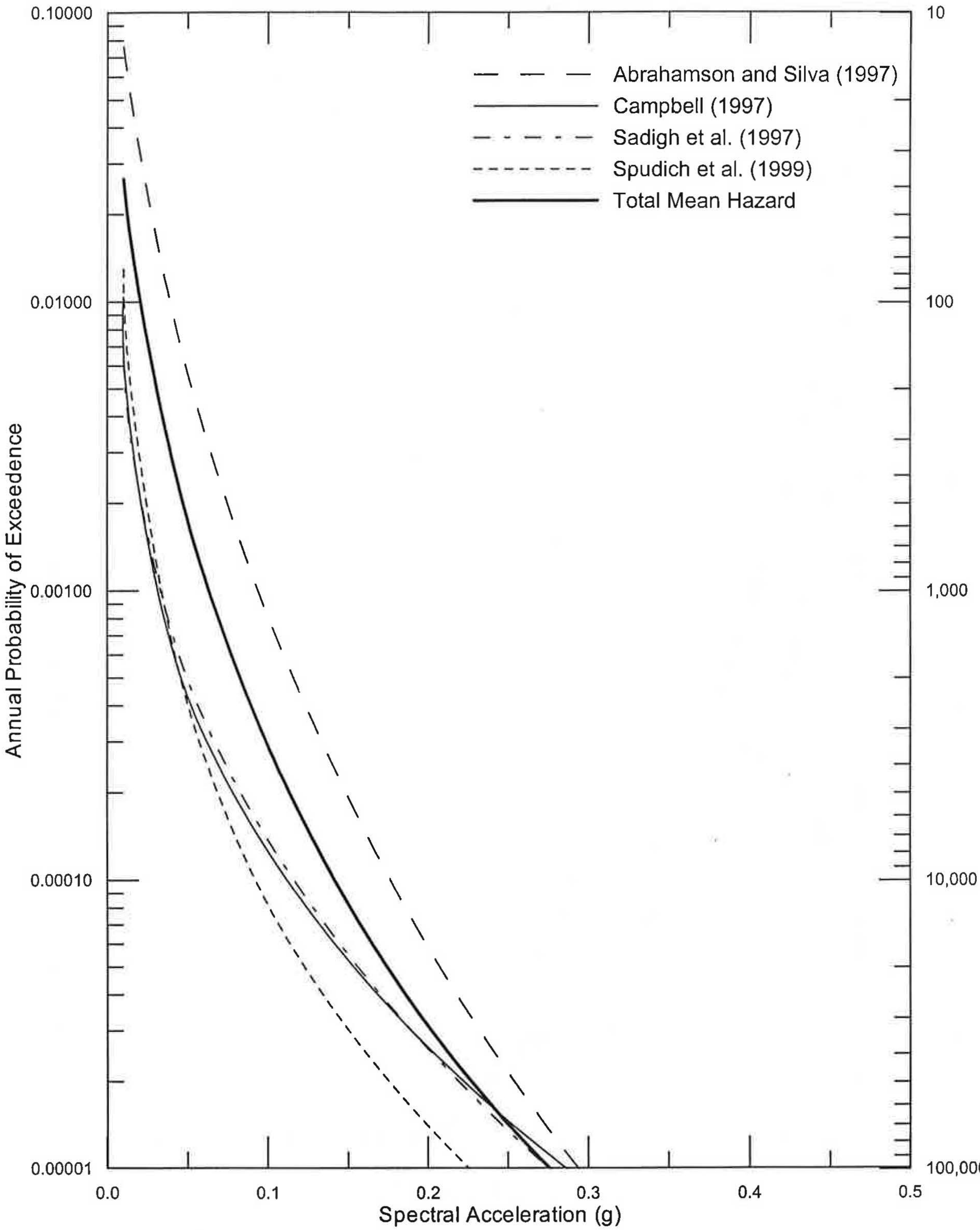

URS	Project No. 68-FUSBR207.00	MEAN 1.0 SEC SPECTRAL ACCELERATION HAZARD: SENSITIVITY TO ATTENUATION RELATIONS FOR GRANITE REEF DAM	Figure 17
	Roosevelt and Granite Reef Dams		

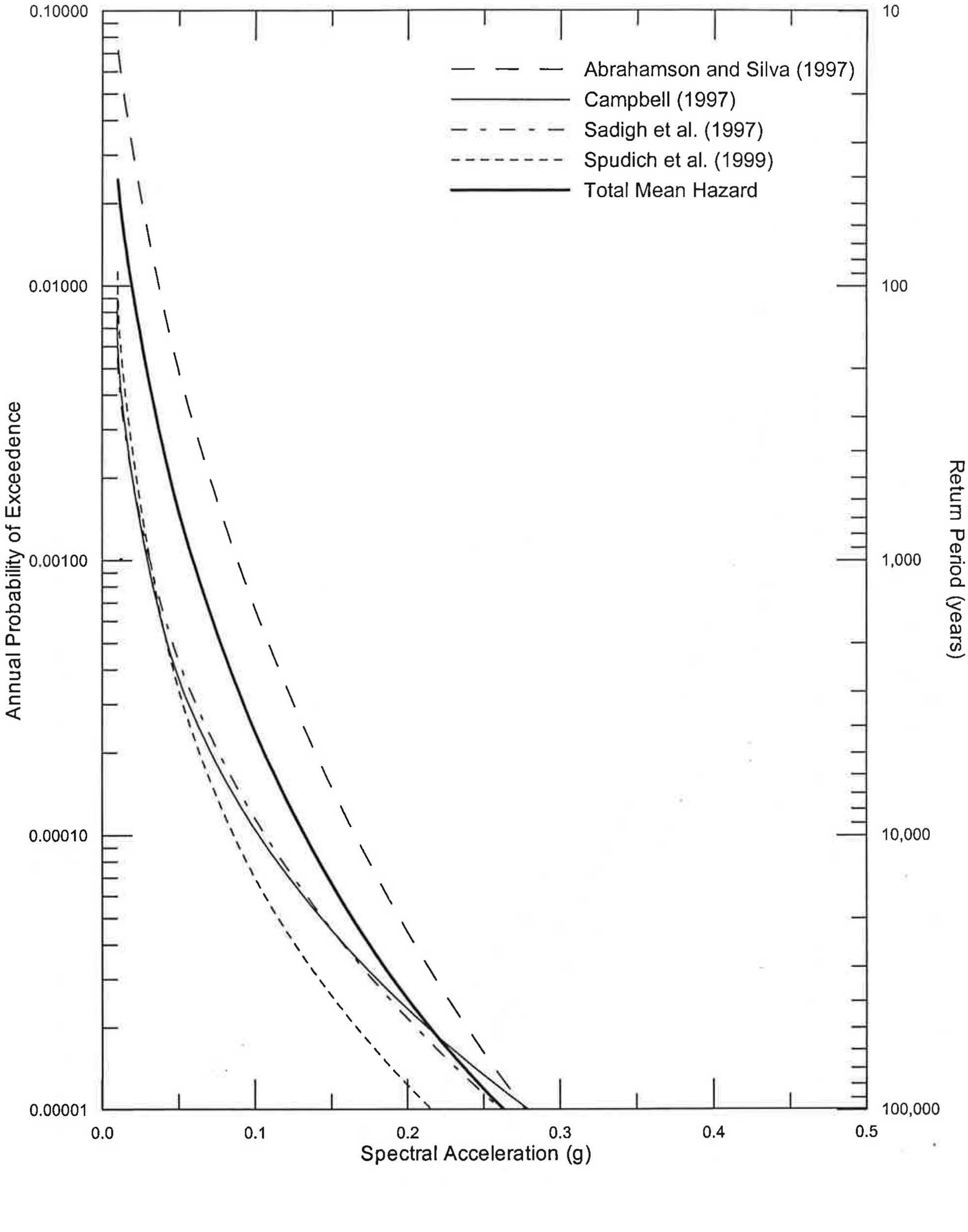

URS	Project No. 68-FUSBR207.00 Roosevelt and Granite Reef Dams	MEAN 1.0 SEC SPECTRAL ACCELERATION HAZARD: SENSITIVITY TO ATTENUATION RELATIONS FOR THEODORE ROOSEVELT DAM	Figure 18

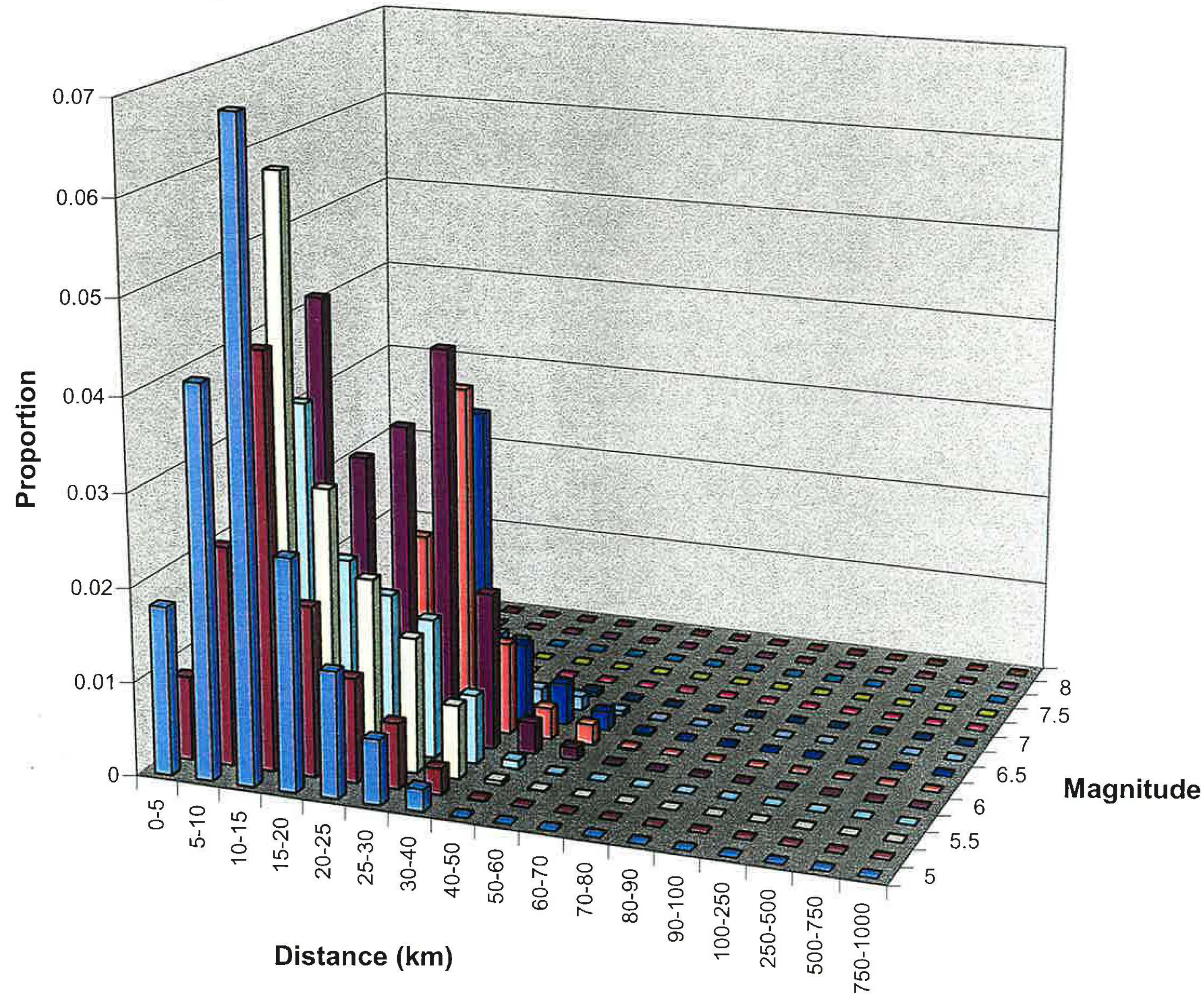

URS	Project No. 68-FUSBR207.00 Roosevelt and Granite Reef Dams	MAGNITUDE AND DISTANCE CONTRIBUTIONS TO THE MEAN PEAK HORIZONTAL ACCELERATION HAZARD AT 10,000 YEARS FOR GRANITE REEF DAM	Figure 19

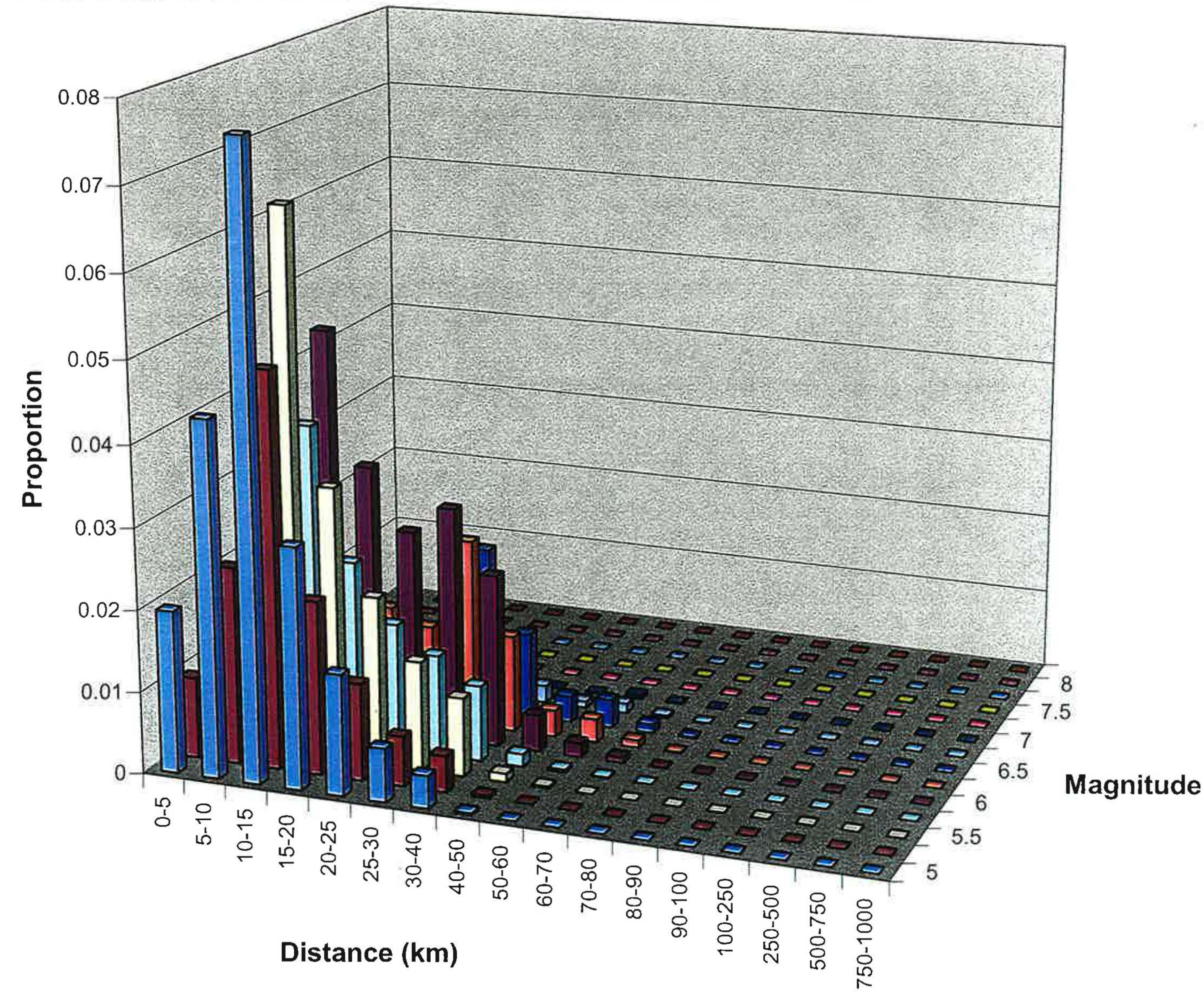

URS	Project No. 68-FUSBR207.00 Roosevelt and Granite Reef Dams	MAGNITUDE AND DISTANCE CONTRIBUTIONS TO THE MEAN PEAK HORIZONTAL ACCELERATION HAZARD AT 10,000 YEARS FOR THEODORE ROOSEVELT DAM	Figure 20

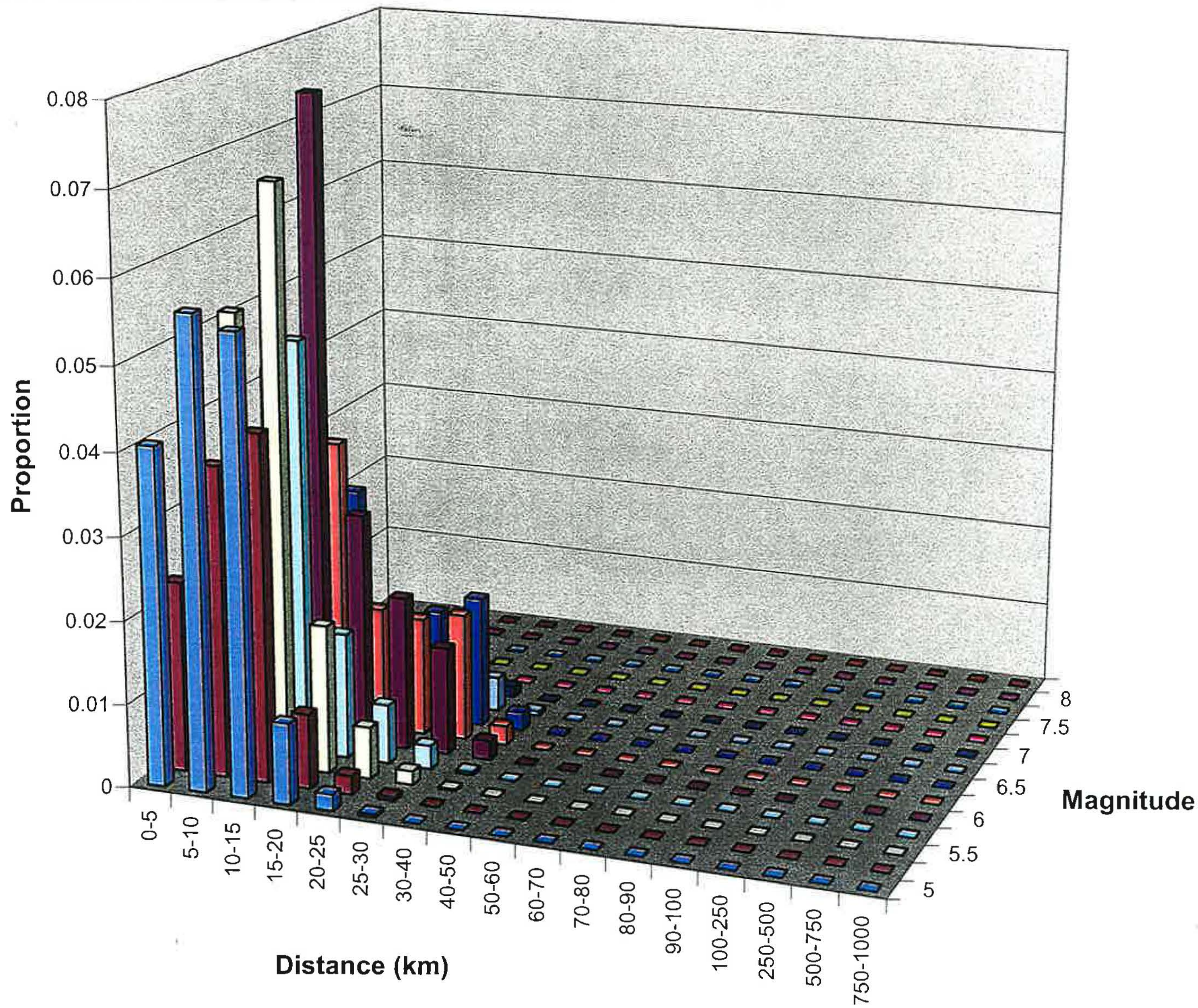

URS	Project No. 68-FUSBR207.00 Roosevelt and Granite Reef Dams	MAGNITUDE AND DISTANCE CONTRIBUTIONS TO THE MEAN PEAK HORIZONTAL ACCELERATION HAZARD AT 50,000 YEARS FOR GRANITE REEF DAM	Figure 21

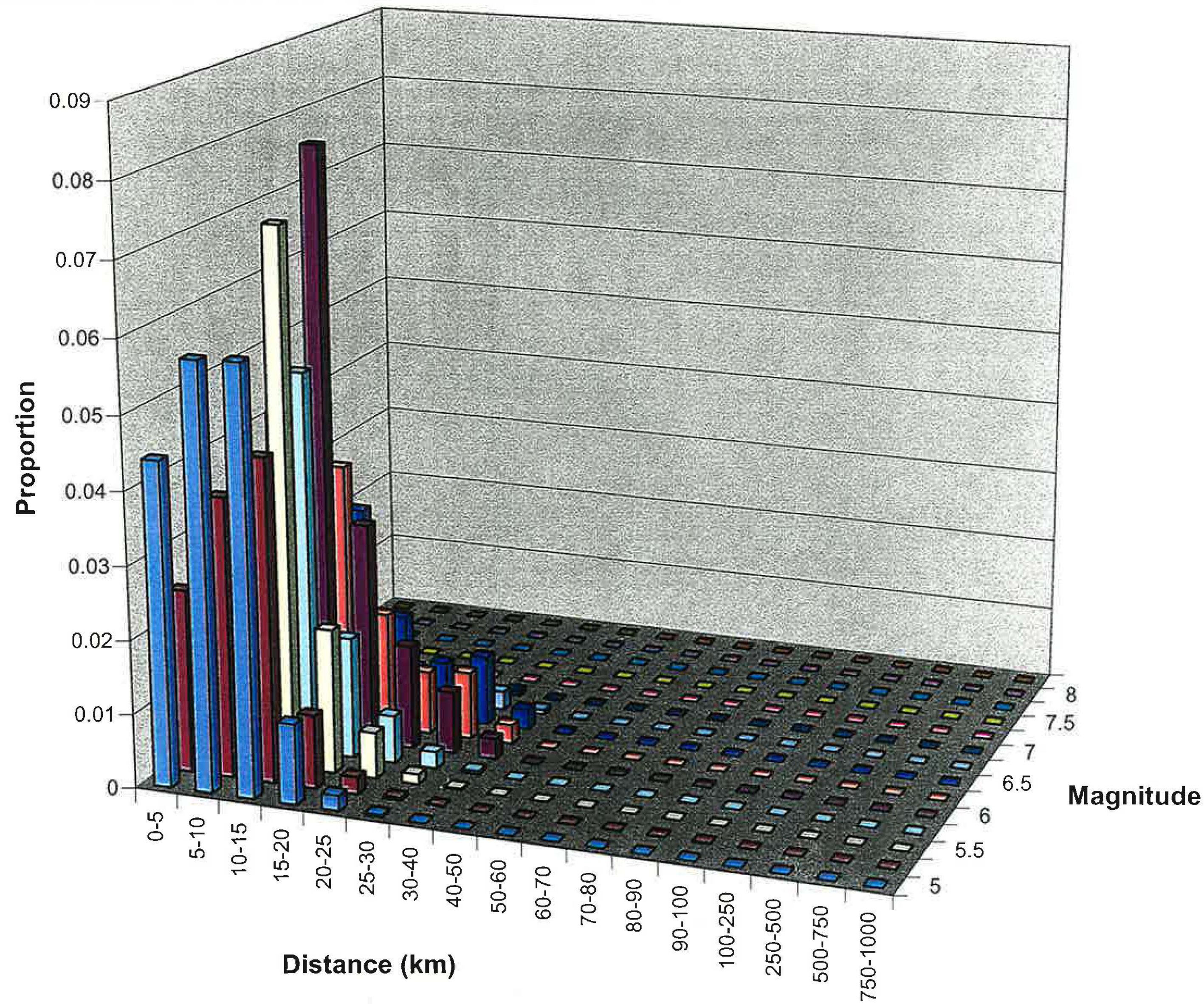

URS

Project No. 68-FUSBR207.00

Roosevelt and Granite Reef Dams

MAGNITUDE AND DISTANCE CONTRIBUTIONS TO THE MEAN PEAK HORIZONTAL ACCELERATION HAZARD AT 50,000 YEARS FOR THEODORE ROOSEVELT DAM

Figure 22

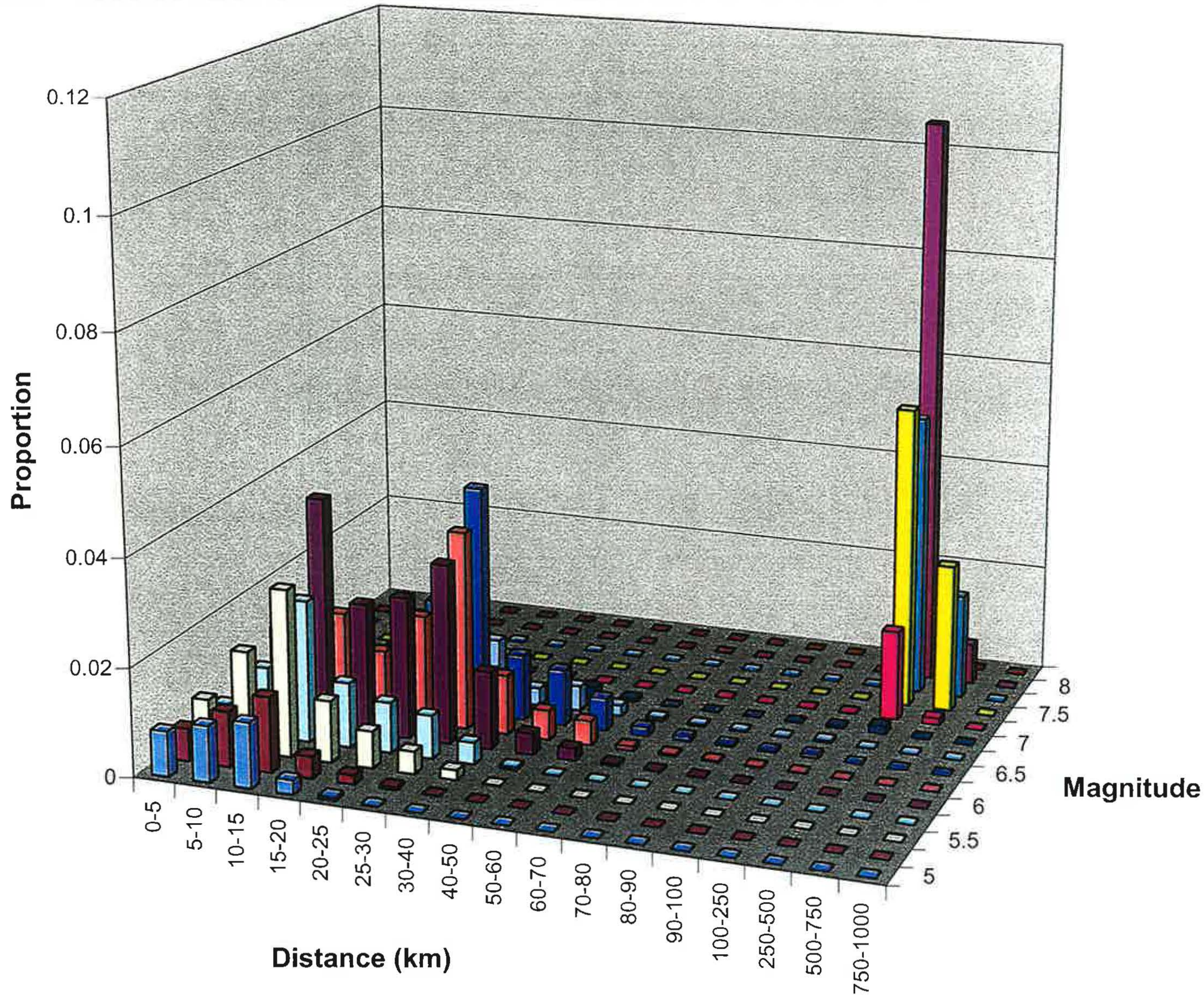

URS	Project No. 68-FUSBR207.00 Roosevelt and Granite Reef Dams	MAGNITUDE AND DISTANCE CONTRIBUTIONS TO THE 1.0 SEC HORIZONTAL SPECTRAL ACCELERATION HAZARD AT 10,000 YEARS FOR GRANITE REEF DAM	Figure 23

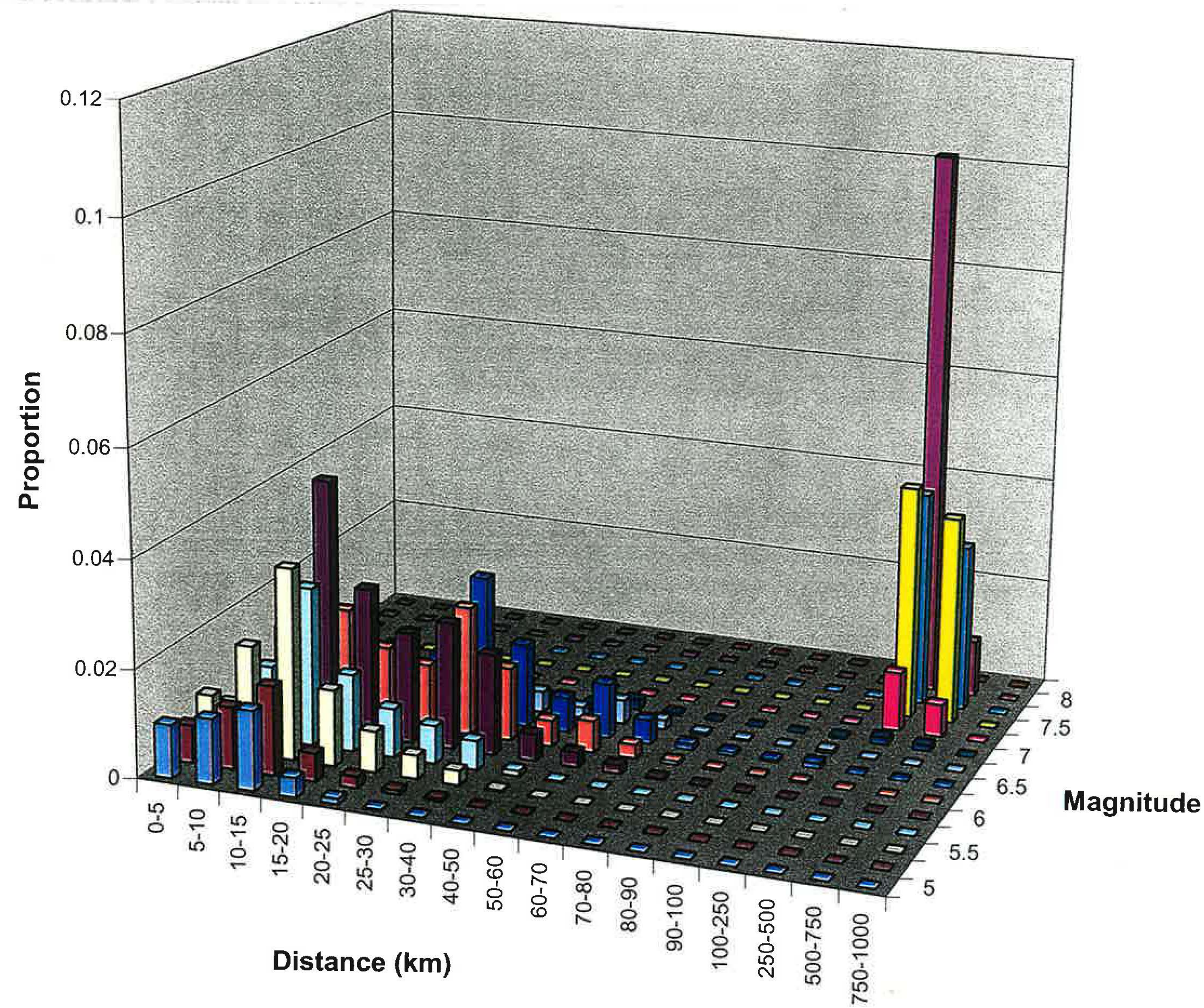

URS	Project No. 68-FUSBR207.00 Roosevelt and Granite Reef Dams	MAGNITUDE AND DISTANCE CONTRIBUTIONS TO THE 1.0 SEC HORIZONTAL SPECTRAL ACCELERATION HAZARD AT 10,000 YEARS FOR THEODORE ROOSEVELT DAM	Figure 24

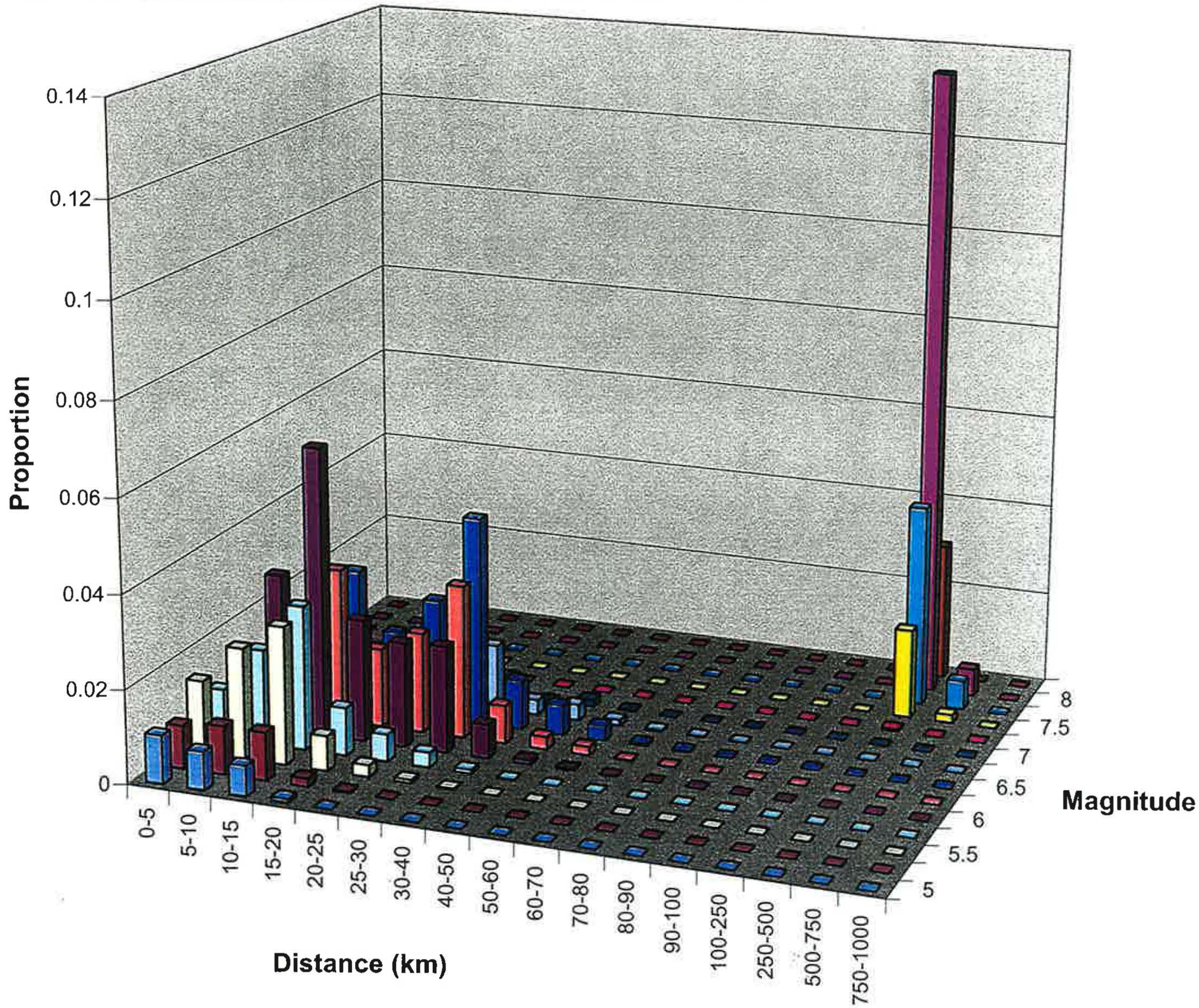

URS	Project No. 68-FUSBR207.00 Roosevelt and Granite Reef Dams	MAGNITUDE AND DISTANCE CONTRIBUTIONS TO THE 1.0 SEC HORIZONTAL SPECTRAL ACCELERATION HAZARD AT 50,000 YEARS FOR GRANITE REEF DAM	Figure 25

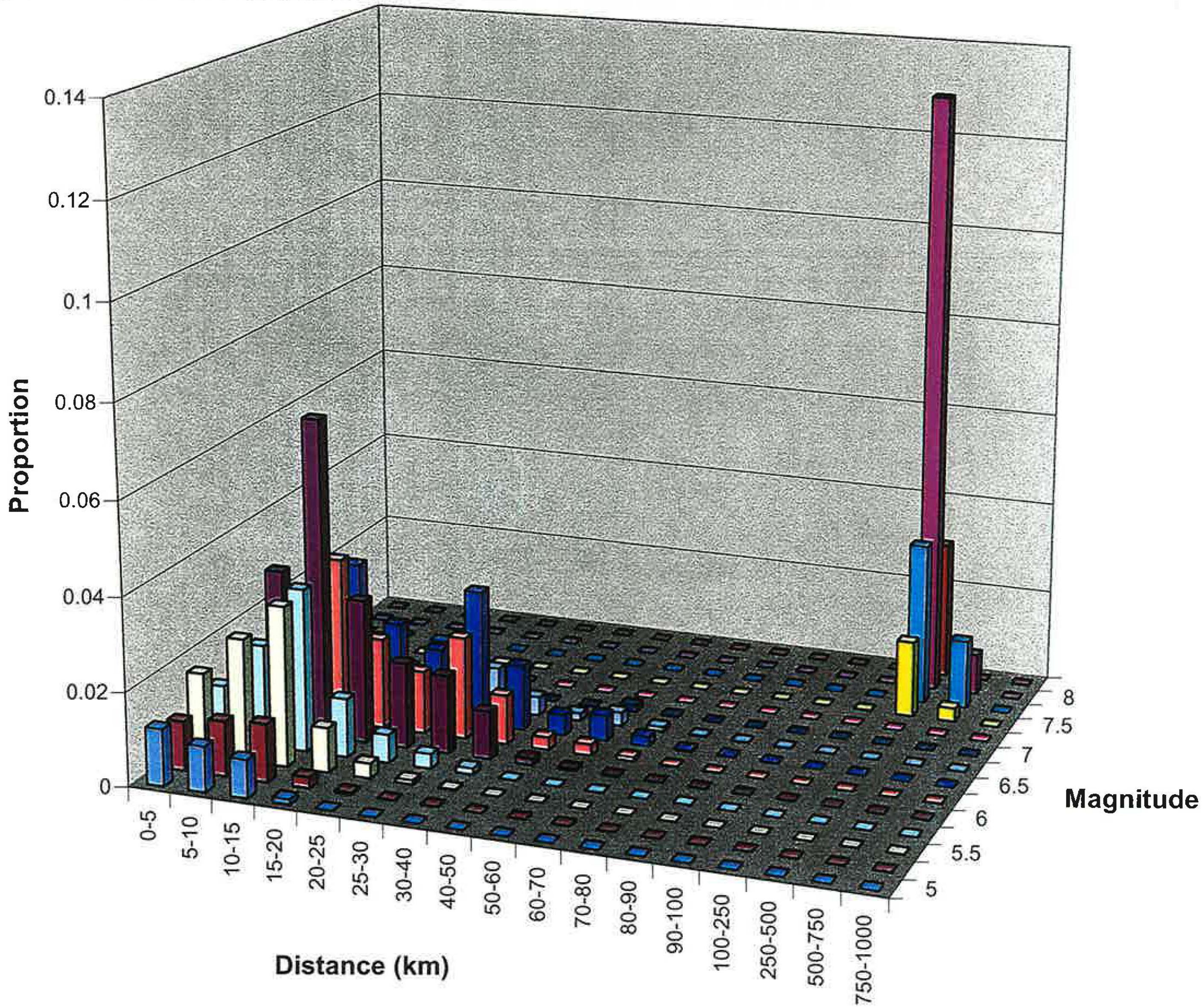

URS	Project No. 68-FUSBR207.00 Roosevelt and Granite Reef Dams	MAGNITUDE AND DISTANCE CONTRIBUTIONS TO THE 1.0 SEC HORIZONTAL SPECTRAL ACCELERATION HAZARD AT 50,000 YEARS FOR THEODORE ROOSEVELT DAM	Figure 26